Supplementary Information for

A peptide ligase and the ribosome cooperate to synthesize the peptide pheganomycin.

Motoyoshi Noike, Takashi Matsui, Koichi Ooya, Ikuo Sasaki, Shouta Ohtaki, Yoshimitsu Hamano, Chitose Maruyama, Jun Ishikawa, Yasuharu Satoh, Hajime Ito, Hiroyuki Morita, and Tohru Dairi*

Supplementary Results

Supplementary Table 1. The proposed functions of each open reading frames.

Gene	Amino acids	Proposed function
-2	195	Hypothetical protein
-1	298	Aldose 1-epimerase
pgm 1	439	Peptide ligase
pgm 2	38	Precursor peptide
pgm 3	656	Radical SAM
pgm 4	385	*C*-methyltransferase
pgm 5	585	ABC transporter
pgm 6	607	ABC transporter
pgm 7	441	Cytochrome P450
pgm 8	436	Aminotransferase
pgm 9	445	DpgC like protein
pgm 10	278	DpgB like protein
pgm 11	353	DpgA like protein
pgm 12	427	Amidinotransferase
pgm 13	746	Hypothetical protein
pgm 14	1159	Peptidase
pgm 15	319	Transcriptional regulator
pgm 16	123	Hypothetical protein
pgm 17	118	Hypothetical protein
pgm 18	427	Permease
pgm 19	441	NRPS C-domain
pgm 20	81	NRPS T-domain
pgm 21	649	NRPS A-domain
+1	247	Dehalogenase/phosphatase
+2	481	MaoC like hydratase

Supplementary Table 2. Conversion ratios of PGM1 reaction.

C-terminus substrates	Conversion ratio (%)*			
	N-terminus substrates			
	4	(*R*)-2-guanidino-2-phenylacetic acid	2-guanidinoacetic acid	creatine
NVKDR	48	44	52	63
NVKDGPT	44			
NV	ND[a]			
NVKDG	41			
NVKDGP	38			
NVKDAGP	45			
QVKDR	32			
NLKDR	49			
NVRDR	42			
DVKDR	13			
FVKDR	32			
AVKDR	38			
NAKDR	26			
NVADR	40			
AAKDR	54			
AAADR	40			
Aspartame	ND[a]			
MRFA (tetra peptide)	ND[a]			
Apidaecin	ND[a]			
Apidaecin derivative	ND[a]			

[a] ND, not determined

***** Consumed substrates (%) were shown.

Average values obtained by two independent experiments are shown. Values were within 7.5 percent of each other.

Supplementary Table 3. Kinetic properties of PGM1.

Substrate	K_m (μM)	k_{cat} (s^{-1})	k_{cat}/K_m (mM^{-1} s^{-1})
4	97 ± 4	26 ± 0.5	268
Peptide (NVKDR)	61 ± 6		426

Triplicate sets of enzyme assays were performed. Data represent mean values ± s.d.

Supplementary Table 4. Relative activity of mutant PGM1 enzymes compared with wild type.

Enzyme	Relative activity (%)*	
	NVKDR	NVKDGPT
Wild type	100	100
A14R	51	55
A14Q	53	54
A14L	95	96
S190L	23	19
S190A	57	55
E255D	16	17
E255S	9.7	7.5
S316D	0.50	0.50
R335M	1.5	2.0
R335Q	1.5	1.7
R335N	1.2	1.1
S339A	7.7	7.6

* Relative activity was normalized by the maximum amount of the product, which was obtained by wild type PGM1 with **2** and NVKDR or NVKDGPT as the substrates.

Average values obtained by two independent experiments are shown. Values were within 8.7 percent of each other.

Supplementary Table 5. Oligonucleotides used in this study.

Primer sequences used for PCR (5' to 3')	Introduced restriction enzyme site	Note
CATATGCGACTTCTCGTCGGAAACGAC CTCGAGGGCCGACAGGGCCGGGGCGAAGAG	*Nde*I *Xho*I	Used for amplification of *pgm1*
TCTAGAACCCACATCTACGAGATCGTC GAATTCTTGCAGTCGAAGGTCTGGAC	*Xba*I *Eco*RI	Used for amplification of an upstream region of *pgm1*
AAGCTTGTAGTCGAAGAAGTAGGCGATC TCTAGACTTCTCGTCGGAAACGACTGG	*Hin*dIII *Xba*I	Used for amplification of a downstream region of *pgm1*
GAATTCCAGGGACAGGTACTTCCCGTCCTC TCTAGACCAGGGAGAGGCCCGGTGTCCTG	*Eco*RI *Xba*I	Used for amplification of an upstream region of *pgm2*
TCTAGACCGTCCCCGGCGAAAGACTTACCG AAGCTTCGCCCGCACCCTCGACTGGGAC	*Xba*I *Hin*dIII	Used for amplification of a downstream region of *pgm2*
GAATTCTGGCGCACATCGAGTTGATCGAC TCTAGAGACCCGGTAGGCCTGCGAGATCGTG	*Eco*RI *Xba*I	Used for amplification of an upstream region of *pgm19*
TCTAGAAGCGAGCTGATGCTCGTCGGCGAG AAGCTTCCACCCGGTAGCCGATCAGGTCG	*Xba*I *Hin*dIII	Used for confirmation of a downstream region of *pgm19*
TAGGCCATGTCCAGGATGTTGTC TGGCCAAGATCATGAACTGCTG		Used for confirmation of *pgm1* disruption
TCCTGGAATCGATGCTCAGTCCGGTA GGATCAGGACAGTGATTGTCTGG		Used for confirmation of *pgm2* disruption
ACGAACTCTCCCACCTCTACTC GTAGAGCATGTTGAGCACCACAC		Used for confirmation of *pgm19* disruption
GCATGCAAGCTTCCTGTGCGTGGAGACGGGCCGCGTCAAC ATGTCTAGAACCTGGCCCGCGCCGAGATGCGGATCG	*Hin*dIII *Xba*I	Used for amplification of 8.9 kb *Hin*dIII-*Xba*I fragment.
ATGTCTAGAGGAGGGCCGGATCTCGGAGCAGGGCTCGCAC ATGTCTAGACAGCCCTGACCGCACGGCCGCTTCGTCGG	*Xba*I *Xba*I	Used for amplification of 7.5 kb *Xba*I-*Xba*I fragment
ATGTCTAGAGGGGCGACCACTCGTCGAAGCTGTGCAGC ATGGAATTCCGACGACGCCGGCGACGCCTATCTGGTC	*Xba*I *Eco*RI	Used for amplification of 7.7 kb *Xba*I-*Eco*RI fragment

Supplementary Table 6. Data collection and refinement statistics.

	PGM1 apo	PGM1-AMP
Data collection		
Space group	*P*1	*P*1
Cell dimensions		
a, *b*, *c* (Å)	77.7, 86.8, 94.3	77.6, 86.7, 94.1
α, β, γ (°)	73.7, 85.9, 68.3	73.9, 86.1, 68.2
Resolution (Å)	50.0-1.95(2.07-1.95) *	50.0-2.17 (2.30-2.17) *
R_{merge}	11.7 (65.3)	11.1 (62.0)
$I / \sigma I$	9.9 (2.3)	5.7 (1.5)
Completeness (%)	96.7 (91.7)	94.5 (90.8)
Redundancy	4.0 (3.9)	2.0 (2.0)
Refinement		
Resolution (Å)	45.18-1.96	45.18-2.18
No. reflections	307,156 (47,097)	66,929 (33,882)
R_{work} / R_{free}	19.4 / 23.1	20.2 / 24.6
No. atoms		
Protein	13,068	12,974
Ligand/ion	87	160
Water	1,299	447
B-factors		
Protein	21.6	39.2
Ligand/ion	35.3	57.2
Water	27.2	39.6
R.m.s. deviations		
Bond lengths (Å)	0.008	0.009
Bond angles (°)	1.060	1.158

*One crystal for each structure was used for data collection and structure determination. Values in parentheses are for the highest resolution shell.

Supplementary Table 7. Grid center and size in each docking simulation.

	grid center			grid size			affinity (kcal/mol)
	x	y	z	x	y	z	
N-terminus substrate							
2	74.5	0	8	6	10	6	-5.3
Peptide							
NVKDR	75.07	-7.085	18.5	21	15	15	-5.2
NVKDGPT	76.604	-7.085	18.263	21	15	13	-5.8

Supplementary Table 8. Oligonucleotides used for construction of mutant enzymes.

Mutant Name	Oligonucleotide sequence
PGM1 A14R	F: 5'-AGGAGCTCCGCGAGCCGACGGGAAGCACGG-3'
	R: 5'-GCTCGCGGAGCTCCTCGCTCCAGTCGTTTC-3'
PGM1 A14Q	F: 5'-AGGAGCTCCAGGAGCCGACGGGAAGCACGG-3'
	R: 5'-GCTCCTGGAGCTCCTCGCTCCAGTCGTTTC-3'
PGM1 A14L	F: 5'-AGGAGCTCCTGGAGCCGACGGGAAGCACGG-3'
	R: 5'-GCTCCAGGAGCTCCTCGCTCCAGTCGTTTC-3'
PGM1 S190L	F: 5'-CGGCTTAGGATCCGACGGCAACGAGATCCTG-3'
	R: 5'-GTCGGATCCTAAGCCGTAGTCCTGTTTGAG-3'
PGM1 S190A	F: 5'-CGGCGCCGGATCCGACGGCAACGAGATCCTG-3'
	R: 5'-GTCGGATCCGGCGCCGTAGTCCTGTTTGAG-3'
PGM1 E255D	F: 5'-GCCTACTTCGCGGACTTCTGGATCTCGGA-3'
	R: 5'-TCCGAGATCCAGAAGTCCGCGAAGTAGGC-3'
PGM1 E255S	F: 5'-CGCGCCTACTTCGCGTCGTTCTGGATCTCGGA-3'
	R: 5'-TCCGAGATCCAGAACGACGCGAAGTAGGCGCG-3'
PGM1 S316D	F: 5'-CGGGGCGTCCTGGACGCGGACGCCGT-3'
	R: 5'-ACGGCGTCCGCGTCCAGGACGCCCCG-3'
PGM1 R335M	F: 5'-ACCGAGCACAACGGCATGGCCACCGGCTCCACC-3'
	R: 5'-GGTGGAGCCGGTGGCCATGCCGTTGTGCTCGGT-3'
PGM1 R335Q	F: 5'-GAGCACAACGGCCAGGCCACCGGCTCCA-3'
	R: 5'-TGGAGCCGGTGGCCTGGCCGTTGTGCTC-3'
PGM1 R335N	F: 5'-CGAGCACAACGGCAATGCCACCGGCTCC-3'
	R: 5'-GGAGCCGGTGGCATTGCCGTTGTGCTCG-3'
PGM1 S339A	F: 5'-CGTGCCACCGGCGCCACCCACATCT-3'
	R: 5'-AGATGTGGGTGGCGCCGGTGGCACG-3'

F, forward primer; R, reverse primer

Mutated codons are underlined.

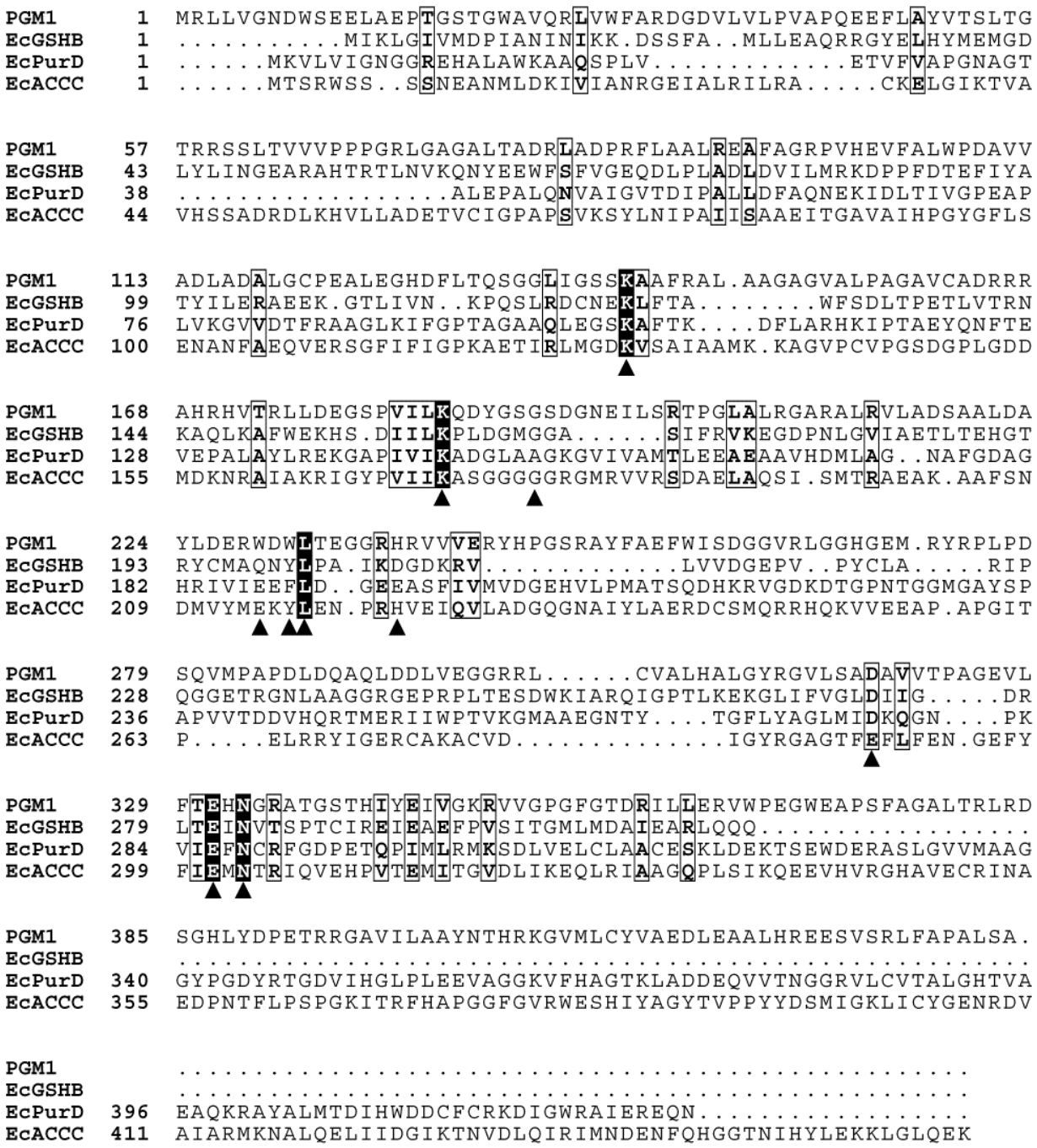

Supplementary Figure 1. Alignment of PGM1 with representative ATP-grasp enzymes. Identical and similar amino acid residues are highlighted by black and white boxes, respectively. The amino acid residues involved in ATP-binding in EcACCC (acetyl-CoA carboxylase subunit A of *E. coli*, accession number, NP_417722) [1] are indicated by solid triangles. EcGSHB: Glutathione synthetase of *E. coli* (NP_417422) [2]; EcPurD: Glycinamide ribonucleotide synthetase of *E. coli* (NP_418433) [3].

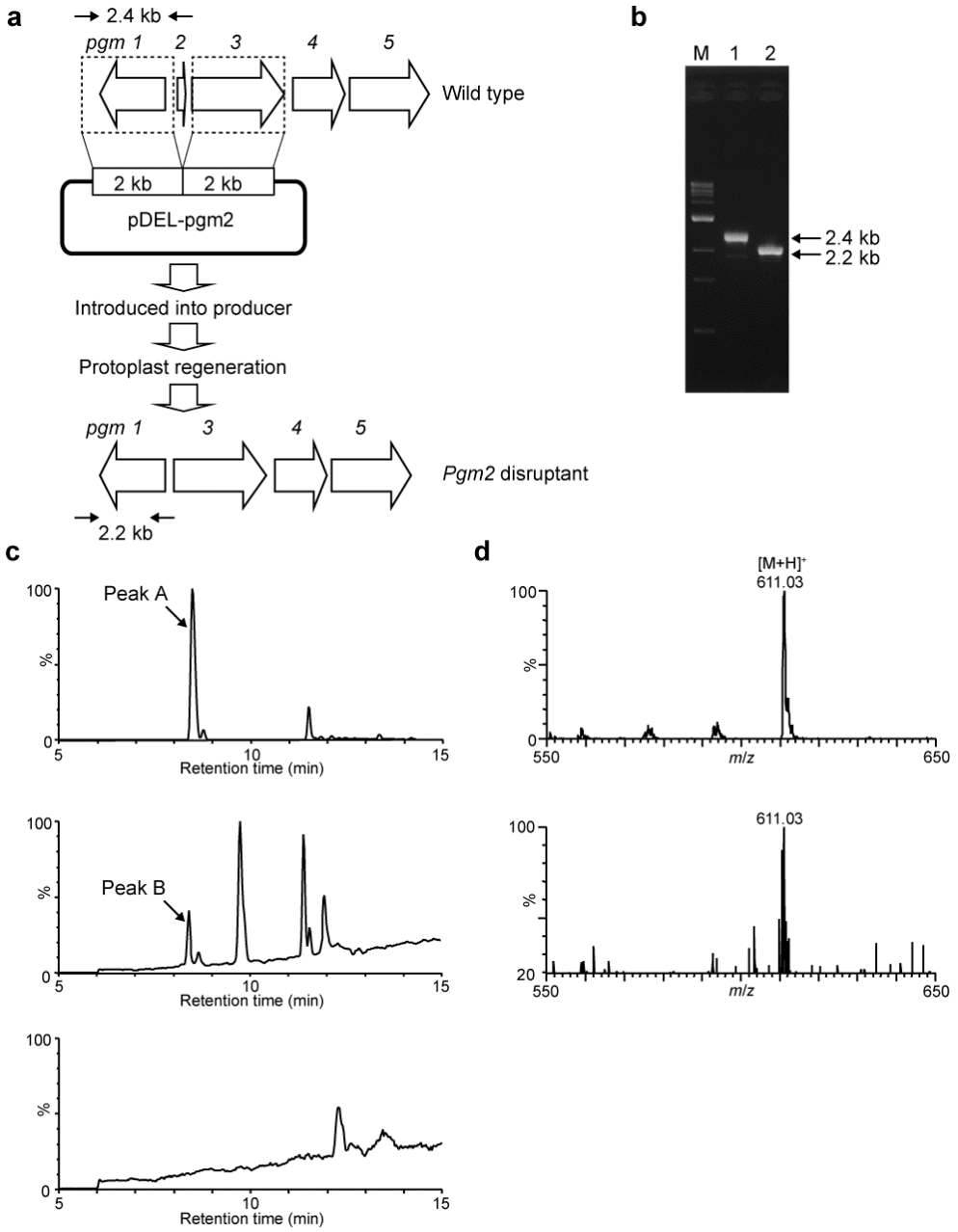

Supplementary Figure 2. Inactivation of *pgm2*. (**a**) A schematic illustration of the strategy for disruption of *pgm2* by a double crossover is shown. Black arrows indicate the primers (Supplementary Table 5) used in PCR analysis, which correspond to the upstream and downstream of *pgm2*. (**b**) Disruption was confirmed by agarose gel electrophoresis of marker (lane M) and the PCR-amplified fragment with genomic DNA of wild (lane 1) and of disruptant (lane 2) as templates. (**c**) LC/ESI-MS analysis of the culture broth. Mass spectra obtained from selected ion chromatograms of the standard of

1 (upper), the products accumulated in the culture broth of wild type (middle), and the *pgm2* mutant (lower) are shown. (**d**) Mass spectra of peak A (upper) and peak B (lower) are shown.

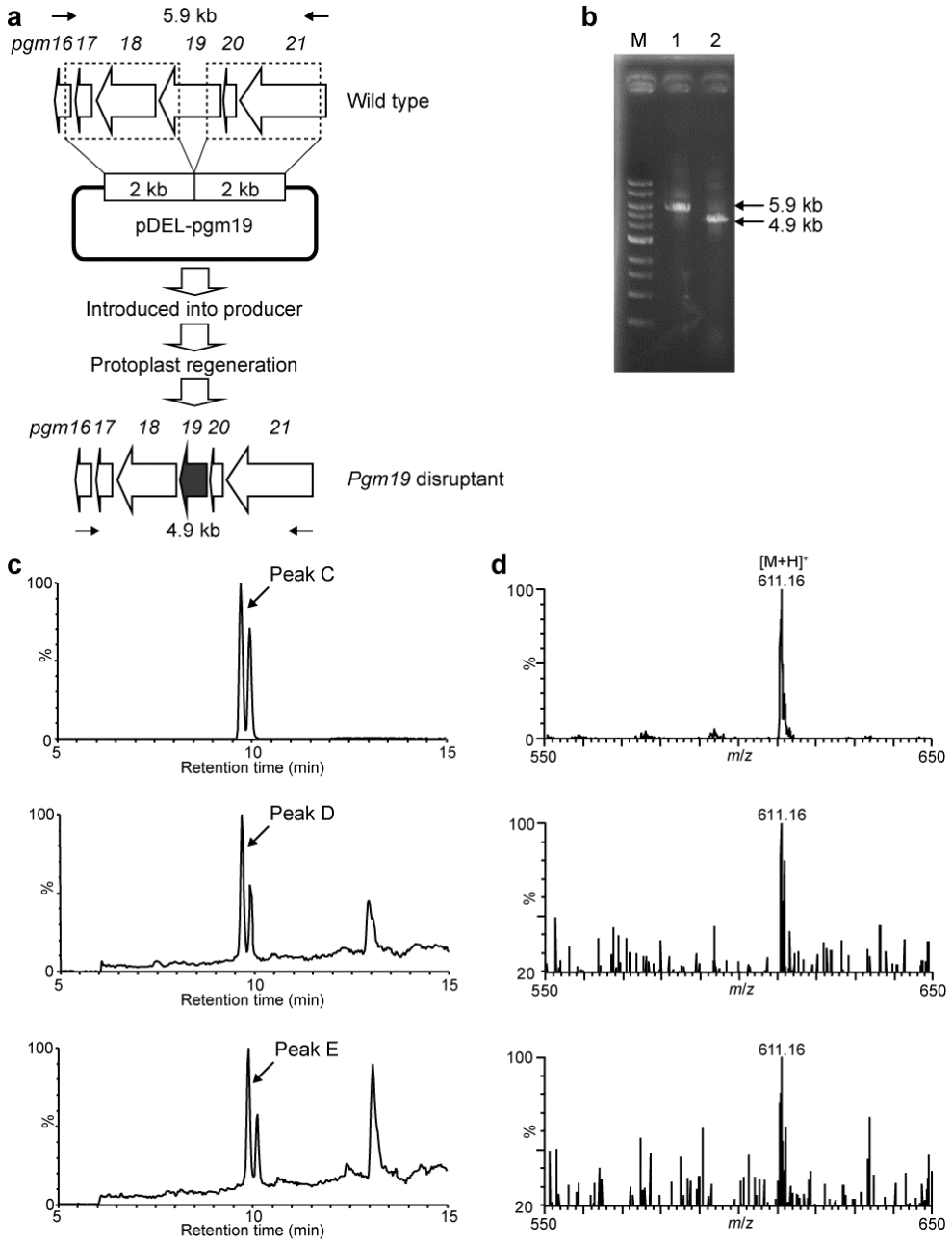

Supplementary Figure 3. Inactivation of *pgm19*. (**a**) The strategy for disruption of *pgm19* by a double crossover is shown. Black arrows indicate the primers (Supplementary Table 5) used in PCR analysis, which correspond to the upstream and downstream of *pgm19*. (**b**) Disruption was confirmed by agarose gel electrophoresis of marker (lane M) and the PCR-amplified fragment with genomic DNA of wild (lane 1) and of disruptant (lane 2) as templates. (**c**) LC/ESI-MS analysis of the culture broth. Mass spectra obtained from selected ion chromatograms of the standard of **1** (upper), the products

accumulated in the culture broth of wild type (middle), and *pgm19* mutant (lower) are shown. (**d**) Mass spectra of peak C (upper), peak D (middle) and peak E (lower) are shown.

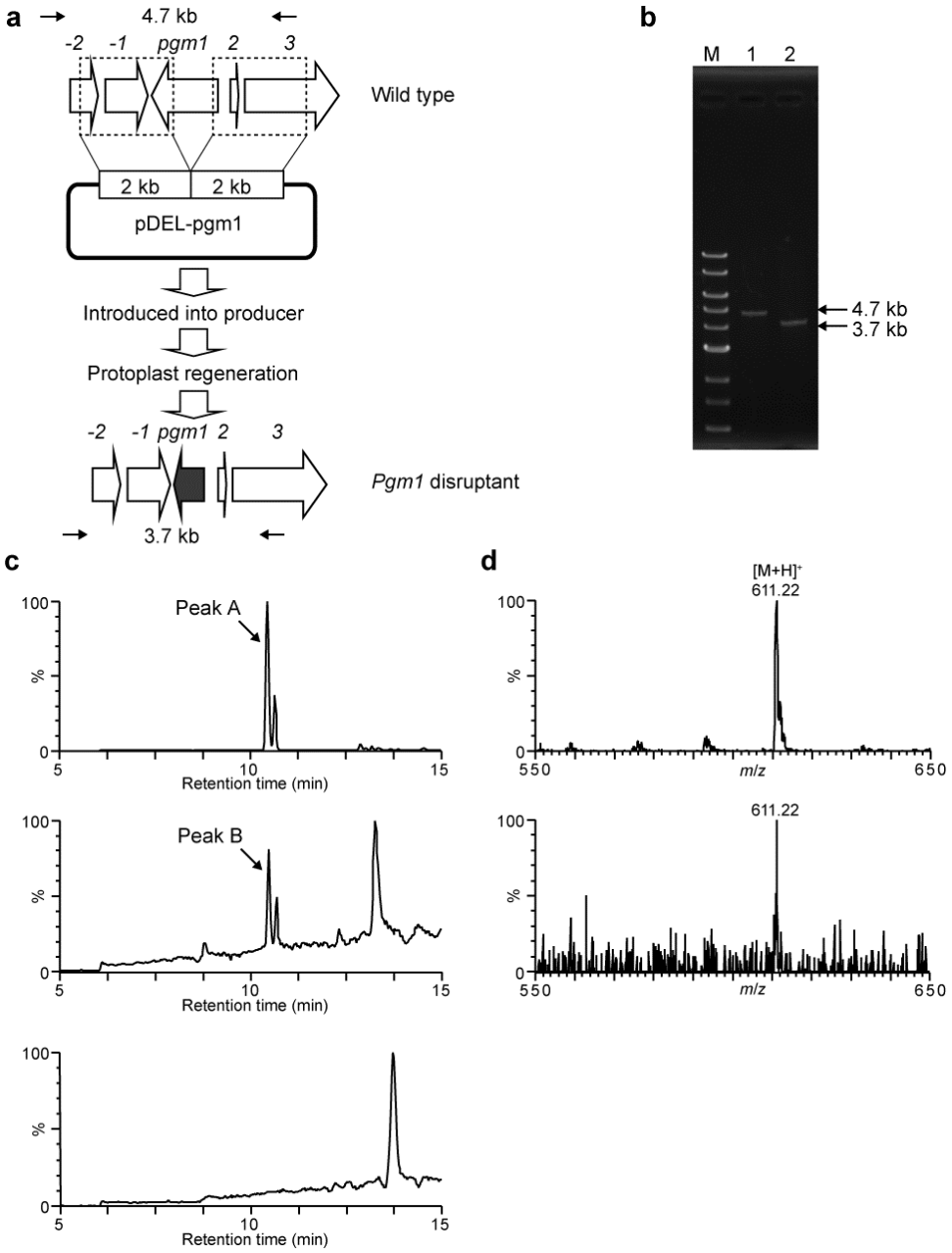

Supplementary Figure 4. Inactivation of *pgm1*. (**a**) A schematic illustration of the strategy for disruption of *pgm1* by a double crossover is shown. Black arrows indicate the primers (Supplementary Table 5) used in PCR analysis, which correspond to the upstream and downstream of *pgm1*. (**b**) Disruption was confirmed by agarose gel electrophoresis of marker (lane M) and the PCR-amplified fragment with genomic DNA of wild (lane 1) and of disruptant (lane 2) as templates. (**c**) LC/ESI-MS analysis of the culture broth. Mass spectra obtained from selected ion chromatograms of the standard of

1 (upper), the products accumulated in the culture broth of wild type (middle), and the *pgm1* mutant (lower) are shown. (**d**) Mass spectra of peak A (upper) and peak B (lower) are shown.

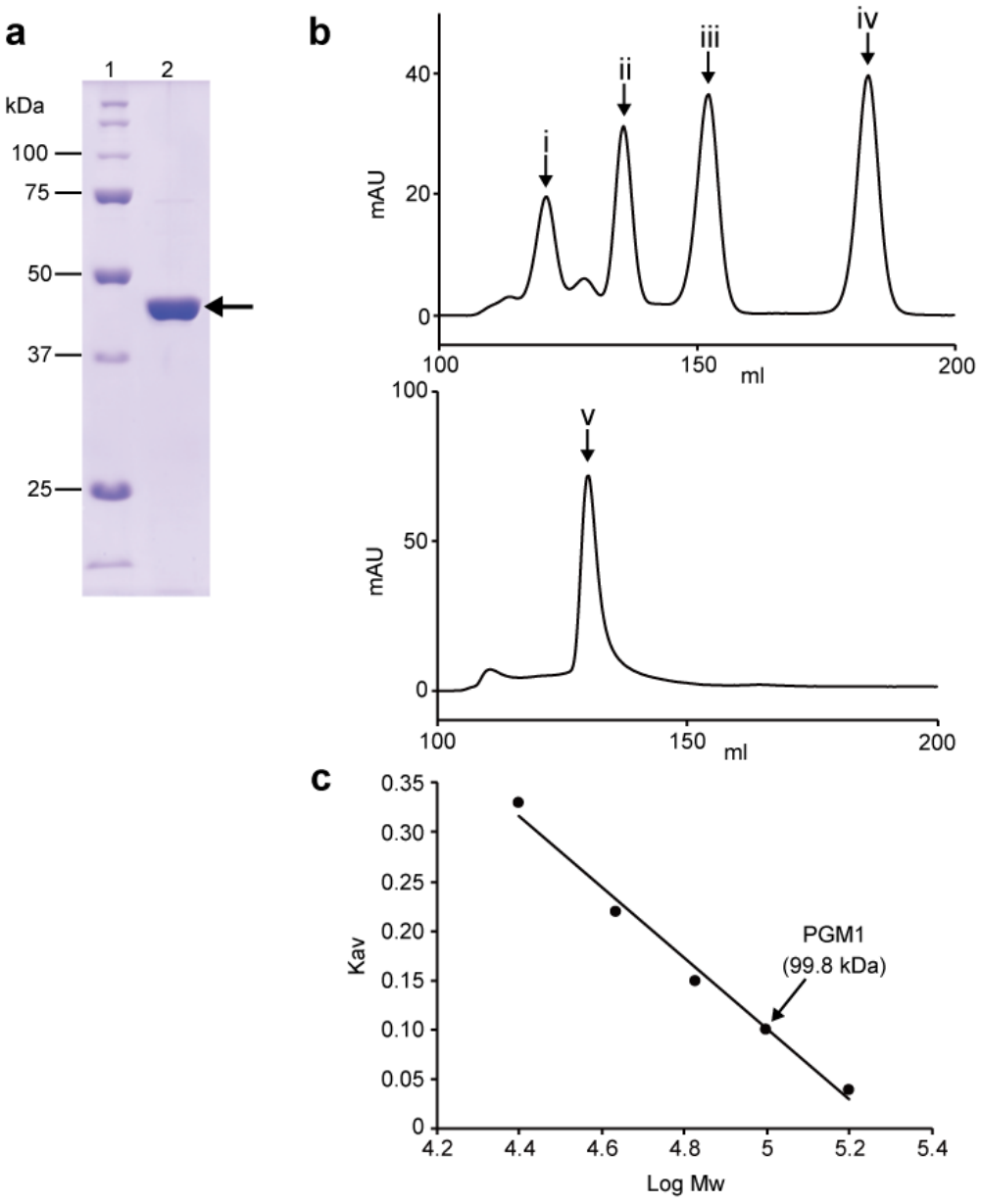

Supplementary Figure 5. Expression and purification of recombinant PGM1. (**a**) SDS-PAGE: molecular mass markers (lane 1) and purified PGM1 (lane 2). (**b**) Gel filtration chromatography: elution profile of the standard proteins aldolase (i, 158 kDa), albumin (ii, 67 kDa), ovalbumin (iii, 43 kDa), chymotrypsinogen A (iv, 25 kDa) and purified PGM1 (bottom, v). (**c**) The *K*av value was defined using the equation $Kav = (Ve - Vo)/(Vc - Vo)$, where V*e*, V*o* and V*c* are the elution, column void, and geometric column volumes, respectively. PGM1 was suggested to be a homodimer.

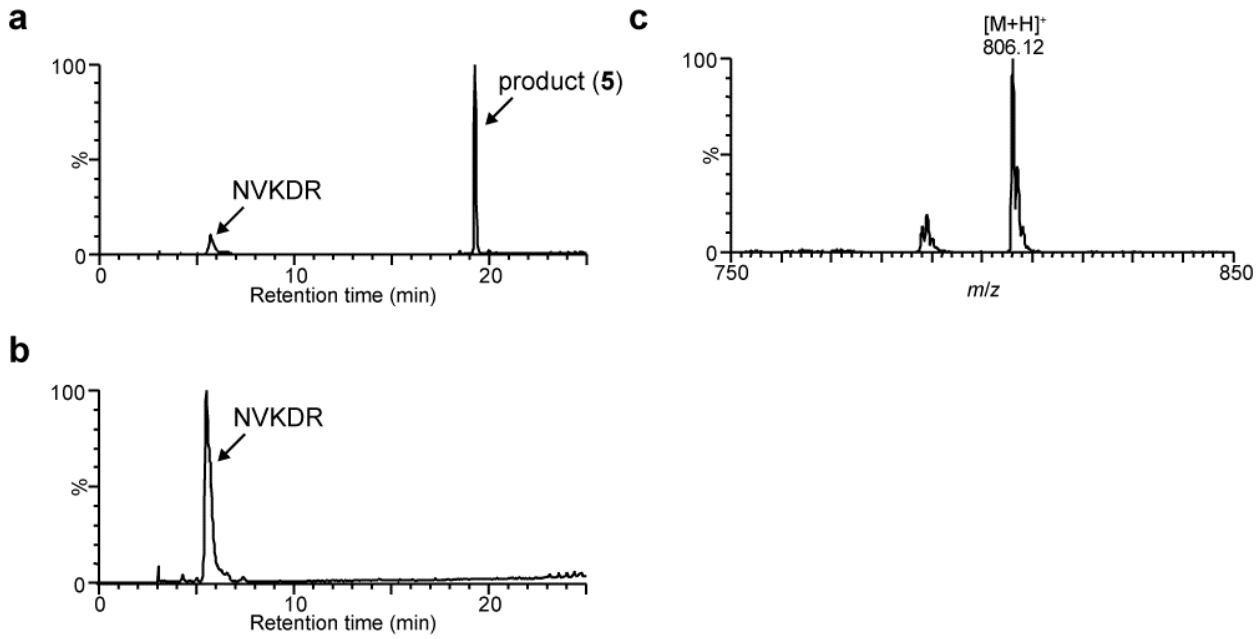

Supplementary Figure 6. LC/ESI-MS analysis of the reaction product. Total ion chromatogram of the reaction product formed from **4** acid and NVKDR with (**a**) and without (**b**) PGM1, and the mass spectrum of the product (**c**) are shown.

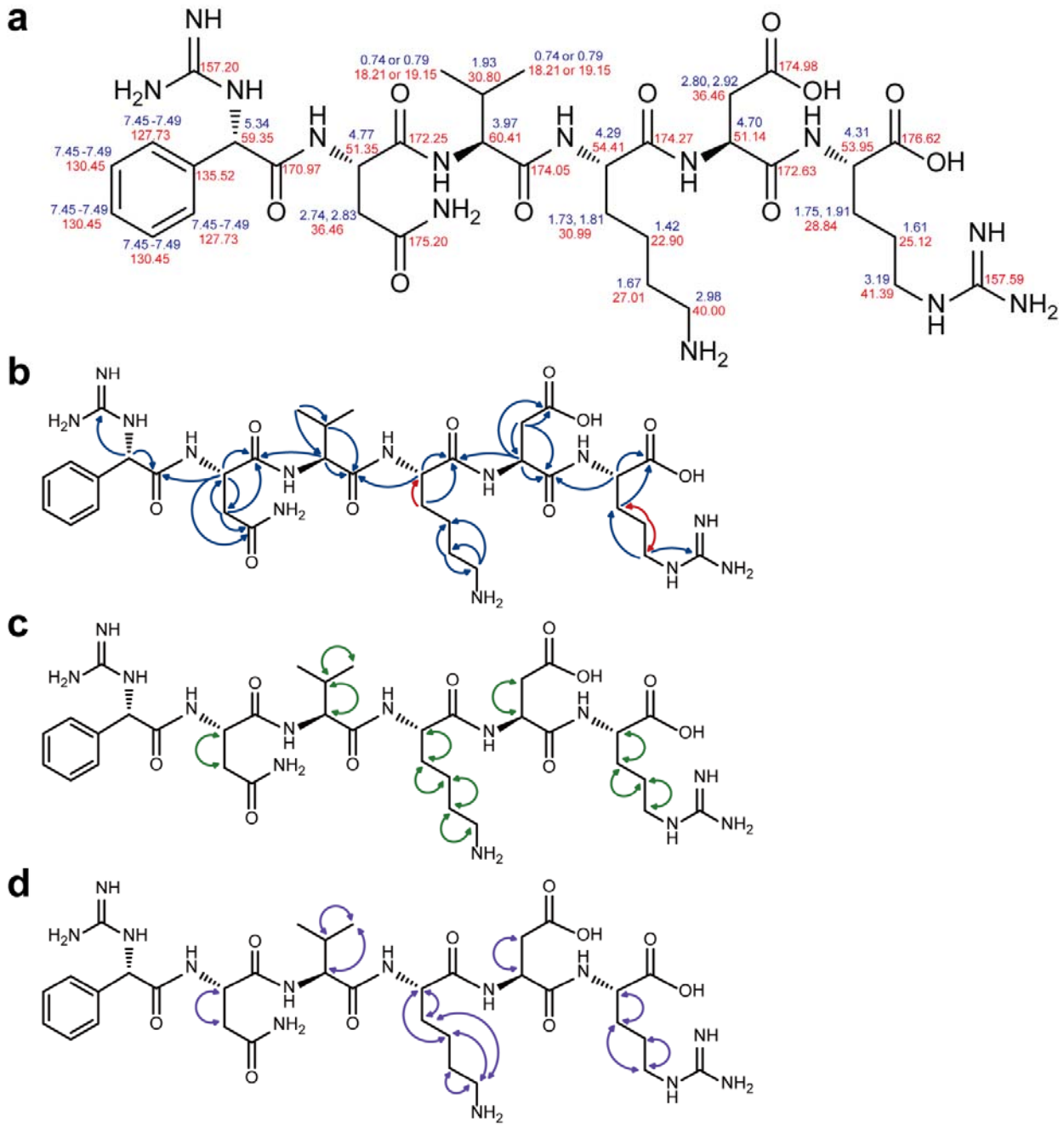

Supplementary Figure 7. NMR analysis of the reaction product formed from 4 and the peptide NVKDR in the presence of PGM1. (**a**) ^{1}H (blue) and ^{13}C (red) NMR spectral data of the reaction product formed from **4** and the peptide NVKDR in the presence of PGM1 in D_2O. (**b**) Selected HMBC (blue arrows) and H_2BC (red arrows) correlations. (**c**) Selected COSY (green arrows) correlations. (**d**) Selected ROESY (purple arrows) correlations.

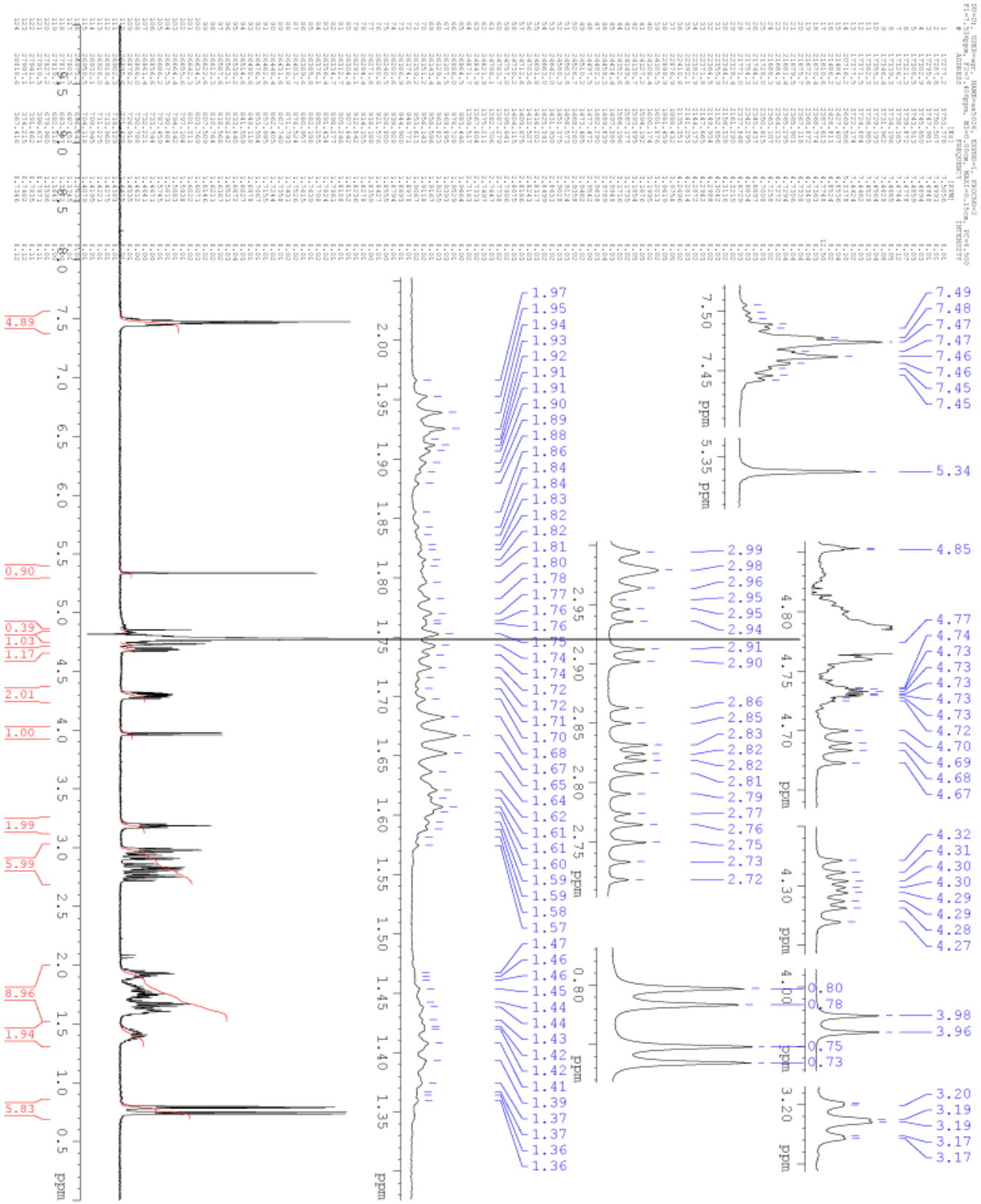

Supplementary Figure 8. ^{1}H NMR of the reaction product formed from 4 and the peptide NVKDR in the presence of PGM1.

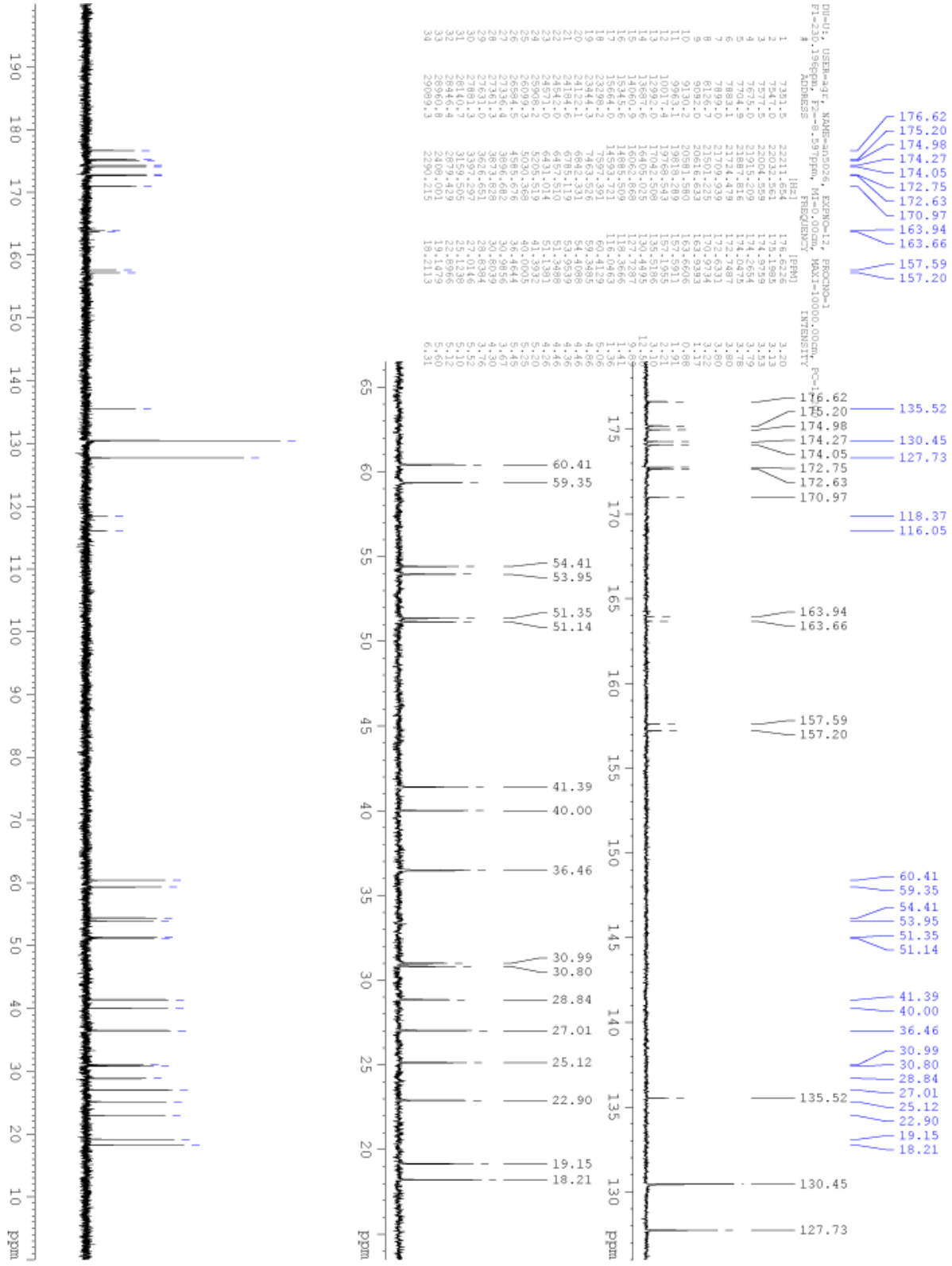

Supplementary Figure 9. ^{13}C NMR of the reaction product formed from 4 and the peptide NVKDR in the presence of PGM1.

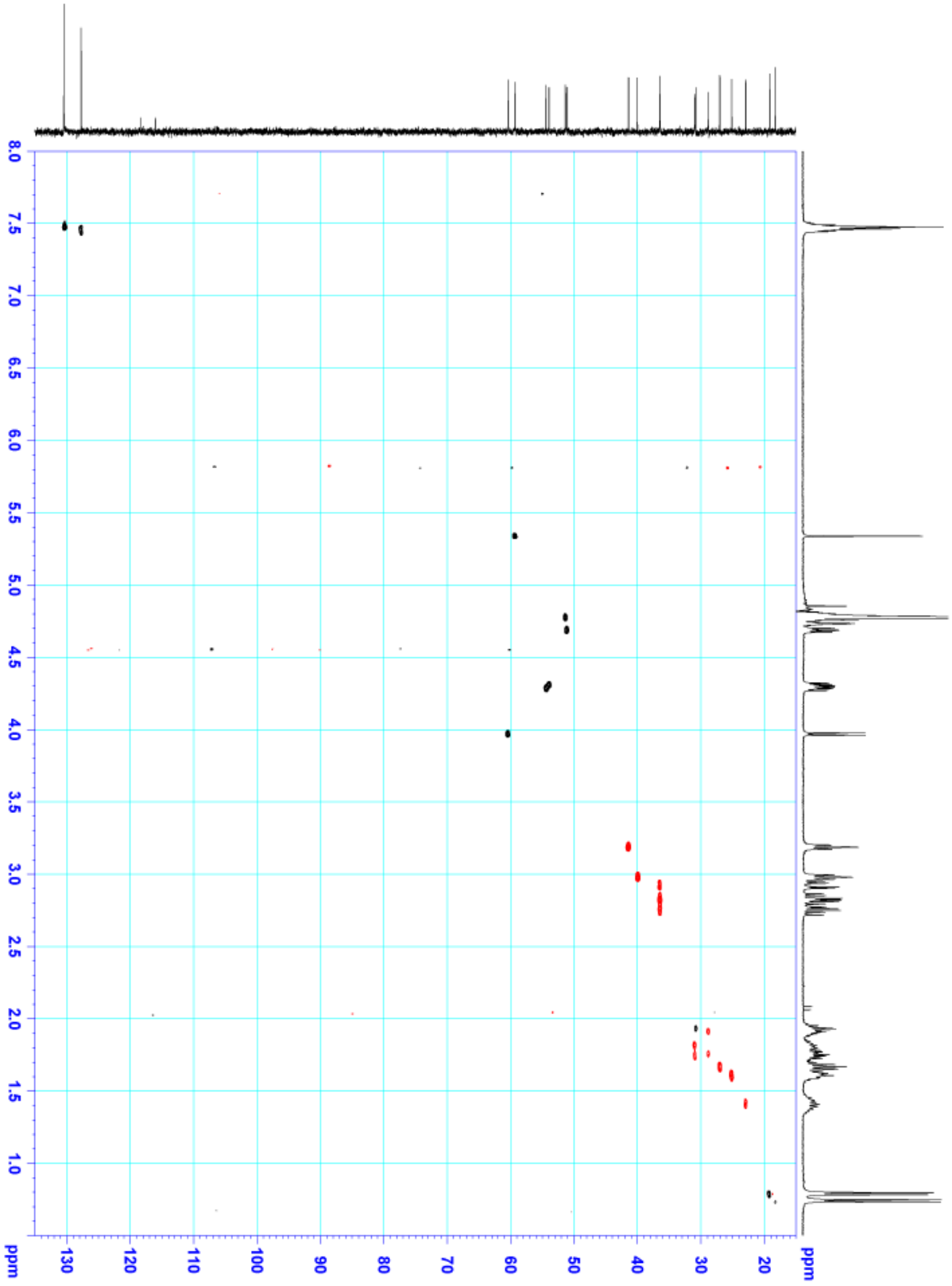

Supplementary Figure 10. HSQC NMR of the reaction product formed from 4 and the peptide NVKDR in the presence of PGM1.

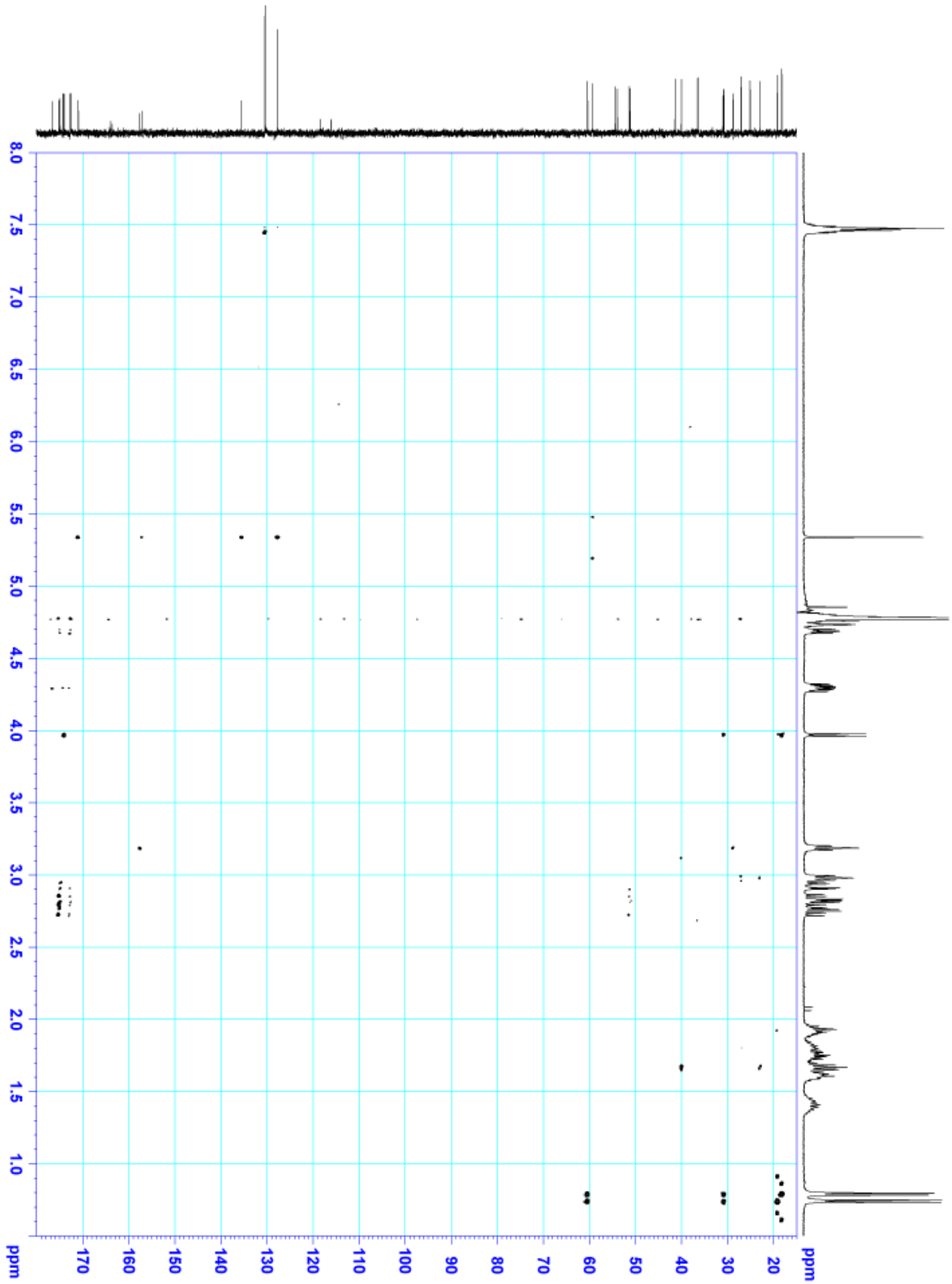

Supplementary Figure 11. HMBC NMR of the reaction product formed from 4 and the peptide NVKDR in the presence of PGM1.

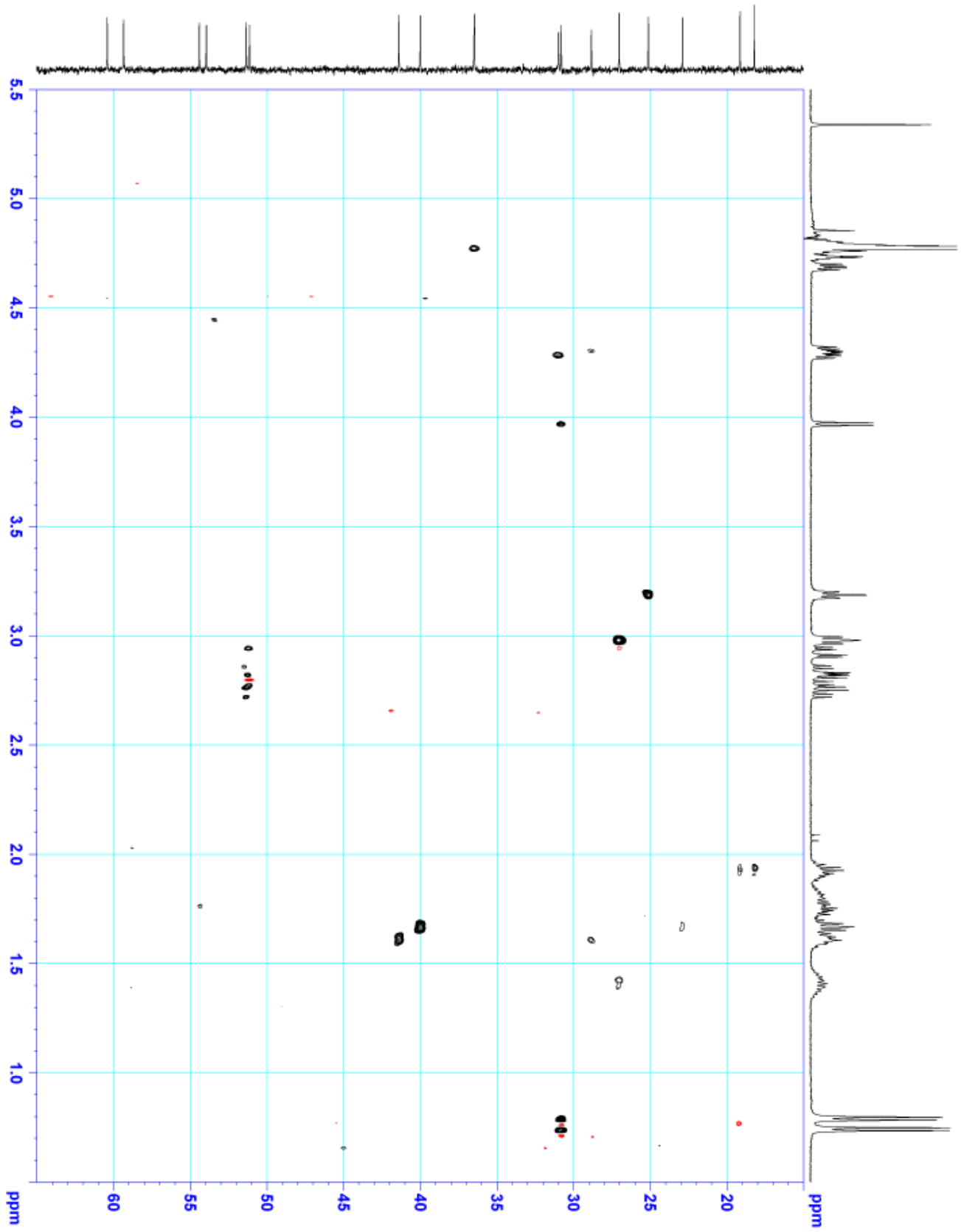

Supplementary Figure 12. H_2BC NMR of the reaction product formed from 4 and the peptide NVKDR in the presence of PGM1.

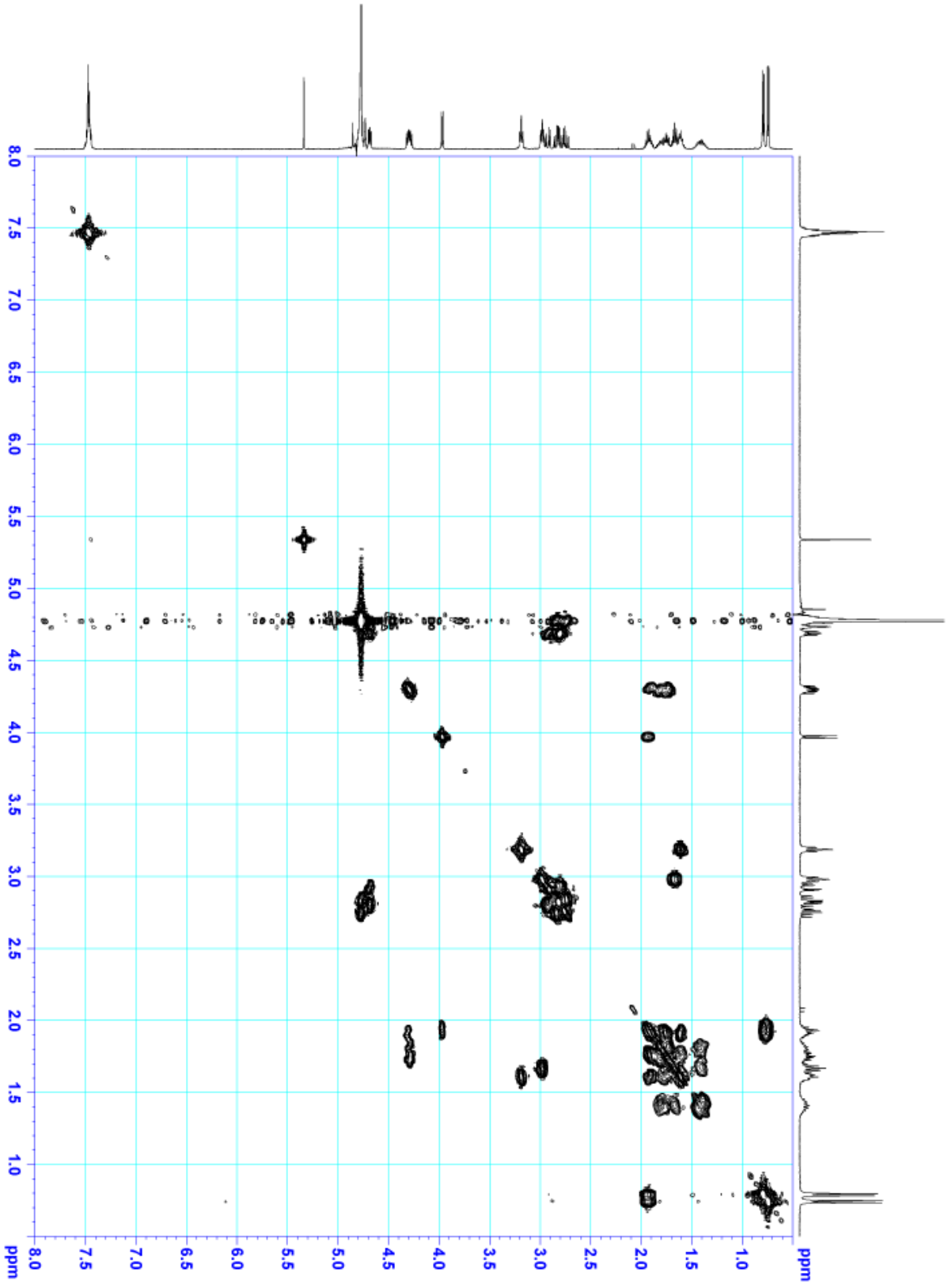

Supplementary Figure 13. COSY NMR of the reaction product formed from 4 and the peptide NVKDR in the presence of PGM1.

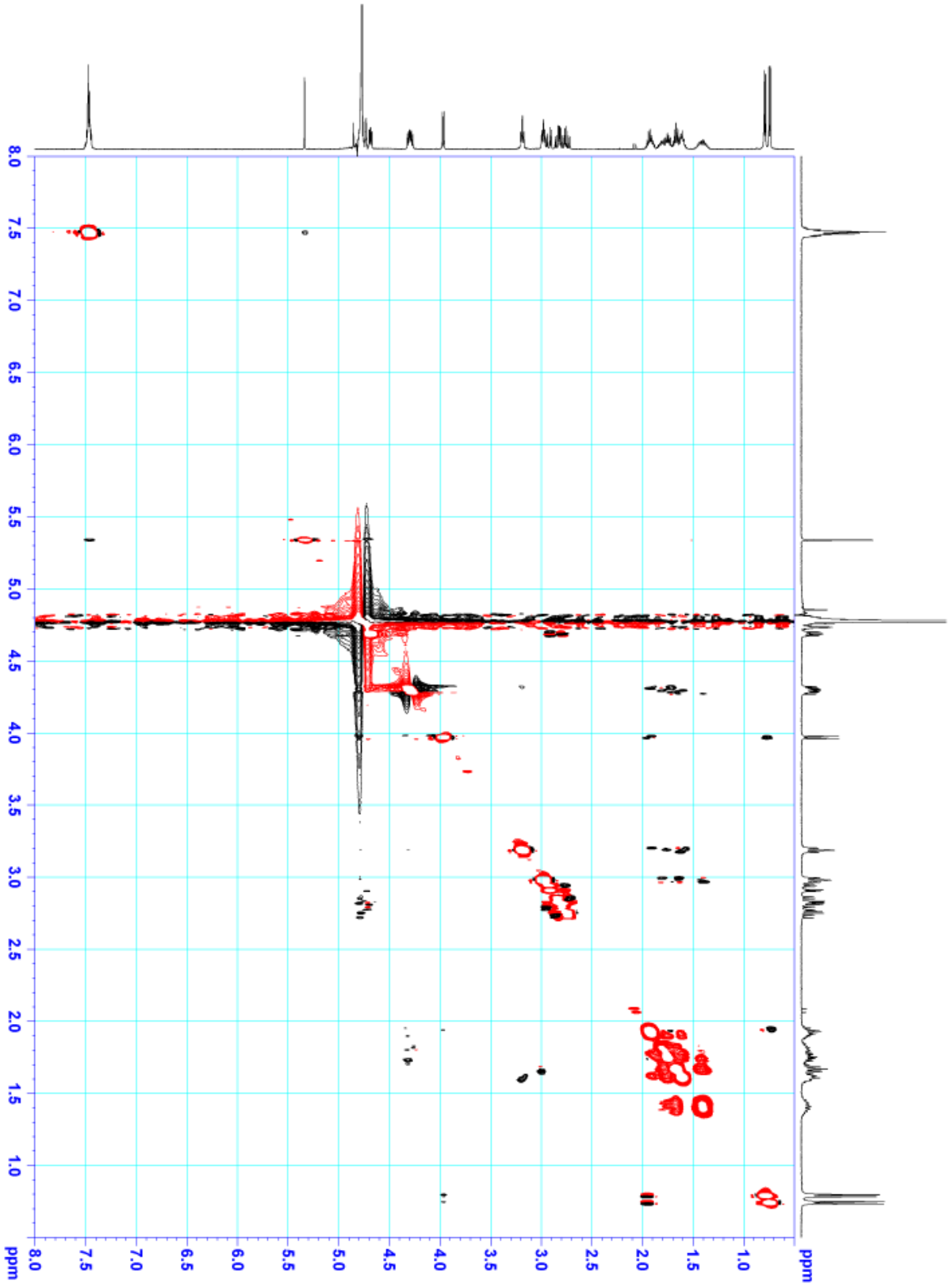

Supplementary Figure 14. ROESY NMR of the reaction product formed from 4 and the peptide NVKDR in the presence of PGM1.

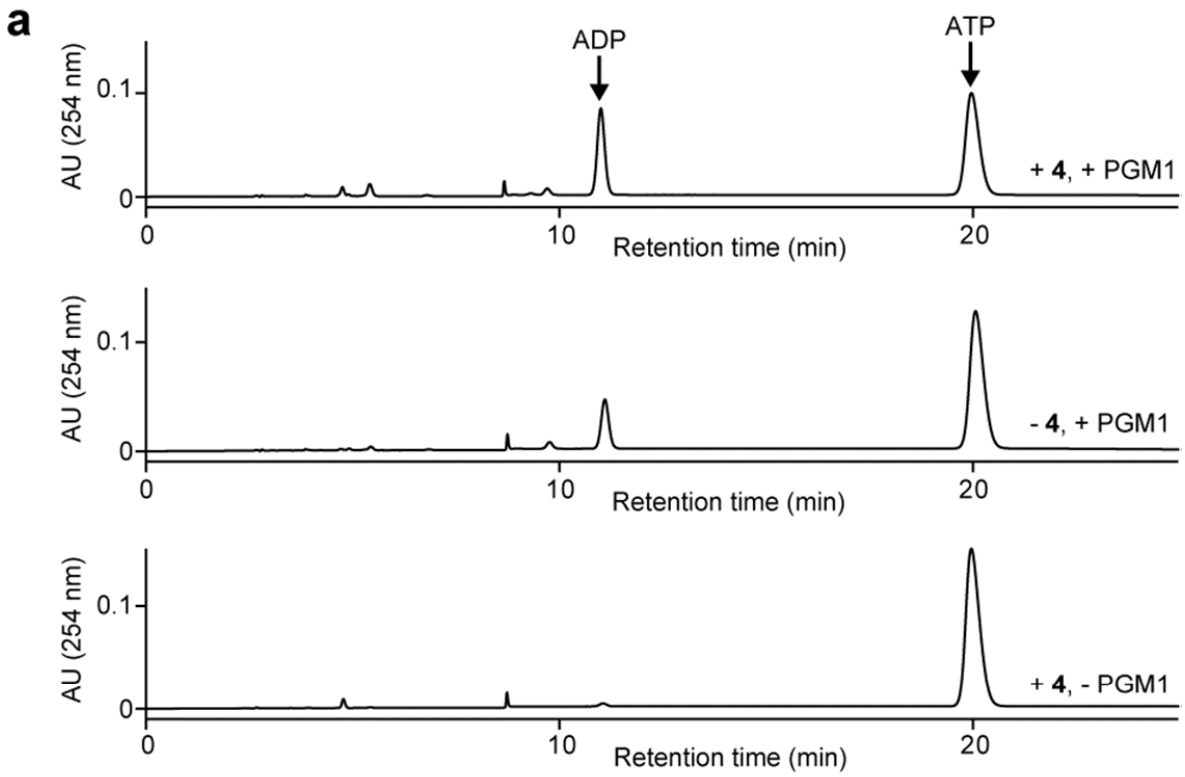
a
ADP
ATP
AU (254 nm)
0.1
0
0
10
20
Retention time (min)
+ 4, + PGM1
- 4, + PGM1
+ 4, - PGM1

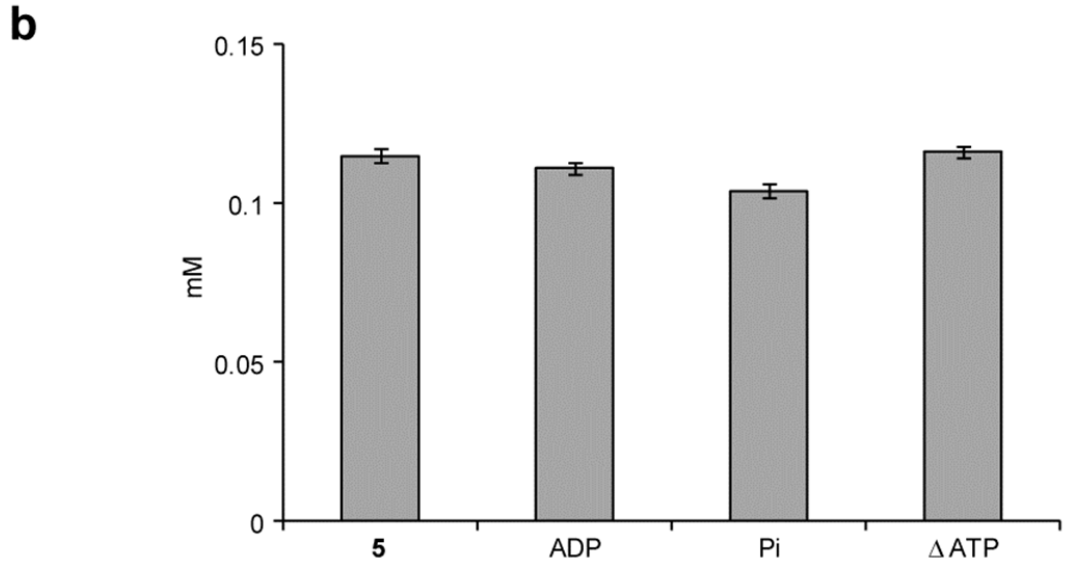
b
0.15
0.1
0.05
0
mM
5
ADP
Pi
ΔATP

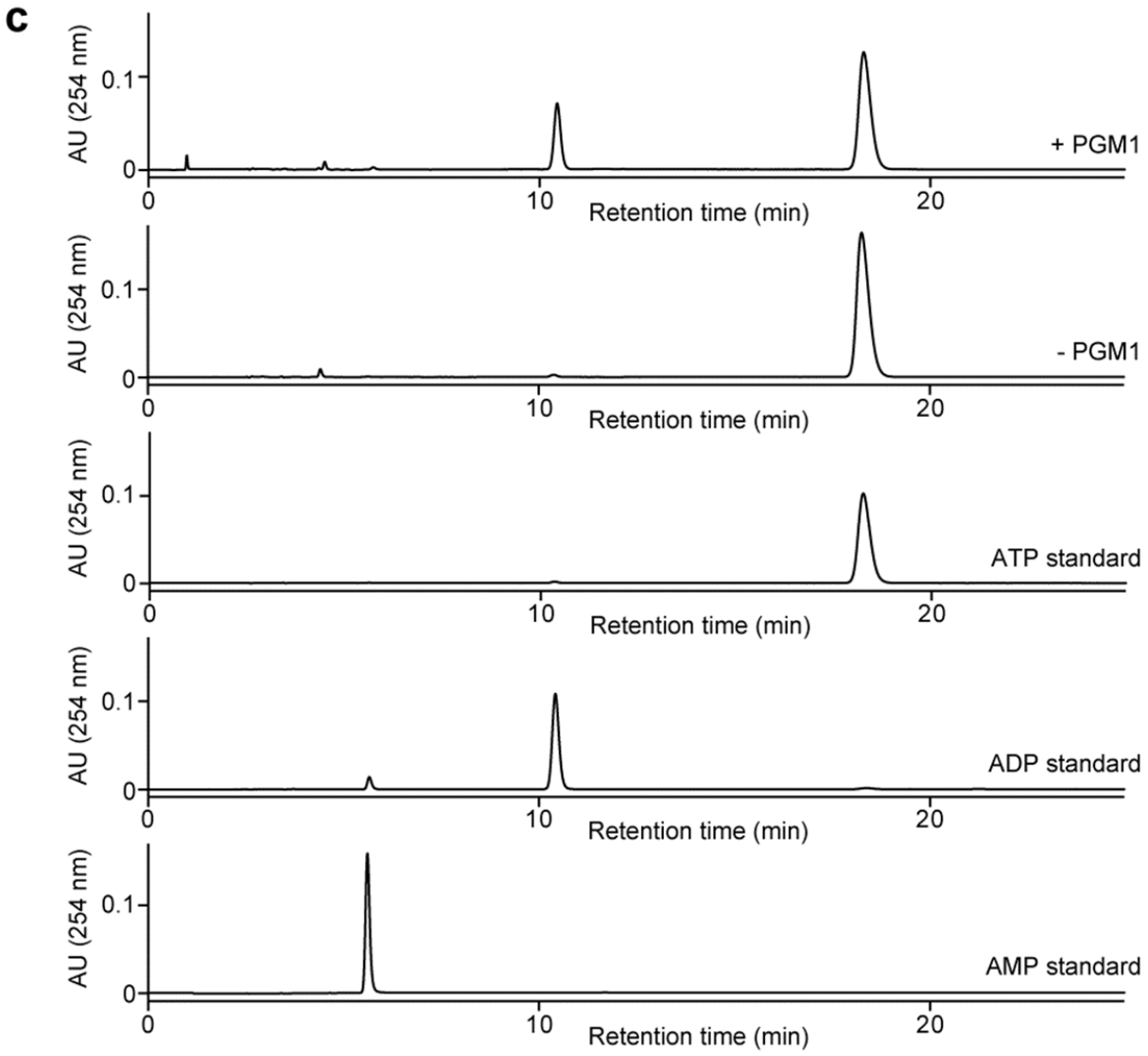

Supplementary Figure 15. Estimation of reaction mechanism of PGM1. (**a**) ADP formed in the reaction mixture containing substrate (**4**) as the sole substrate was quantitatively measured by HPLC. Concentration of ADP was calculated by average values obtained by two independent experiments. (**b**) The formation of **5**, ADP and Pi, and the consumption of ATP were quantitatively measured. Triplicate sets of enzyme assays were performed. Error bars mean values ± s.d. (**c**) ATP consumed and ADP formed during the enzyme reaction were determined by HPLC. The assay and HPLC conditions, and the analytical method for the released Pi are described in the Methods section.

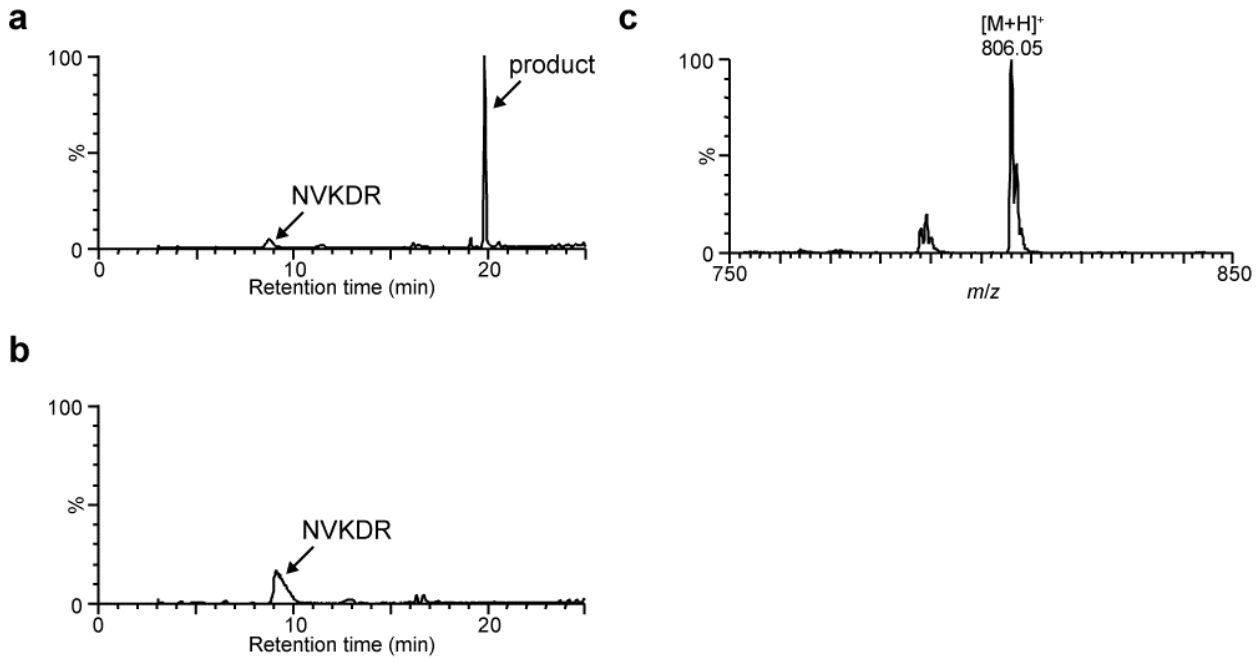

Supplementary Figure 16. LC/ESI-MS analysis of the reaction product. Total ion chromatogram of the reaction product formed from (*R*)-2-guanidino-2-phenylacetic acid and NVKDR with (**a**) and without (**b**) PGM1, and the mass spectrum of the product (**c**) are shown.

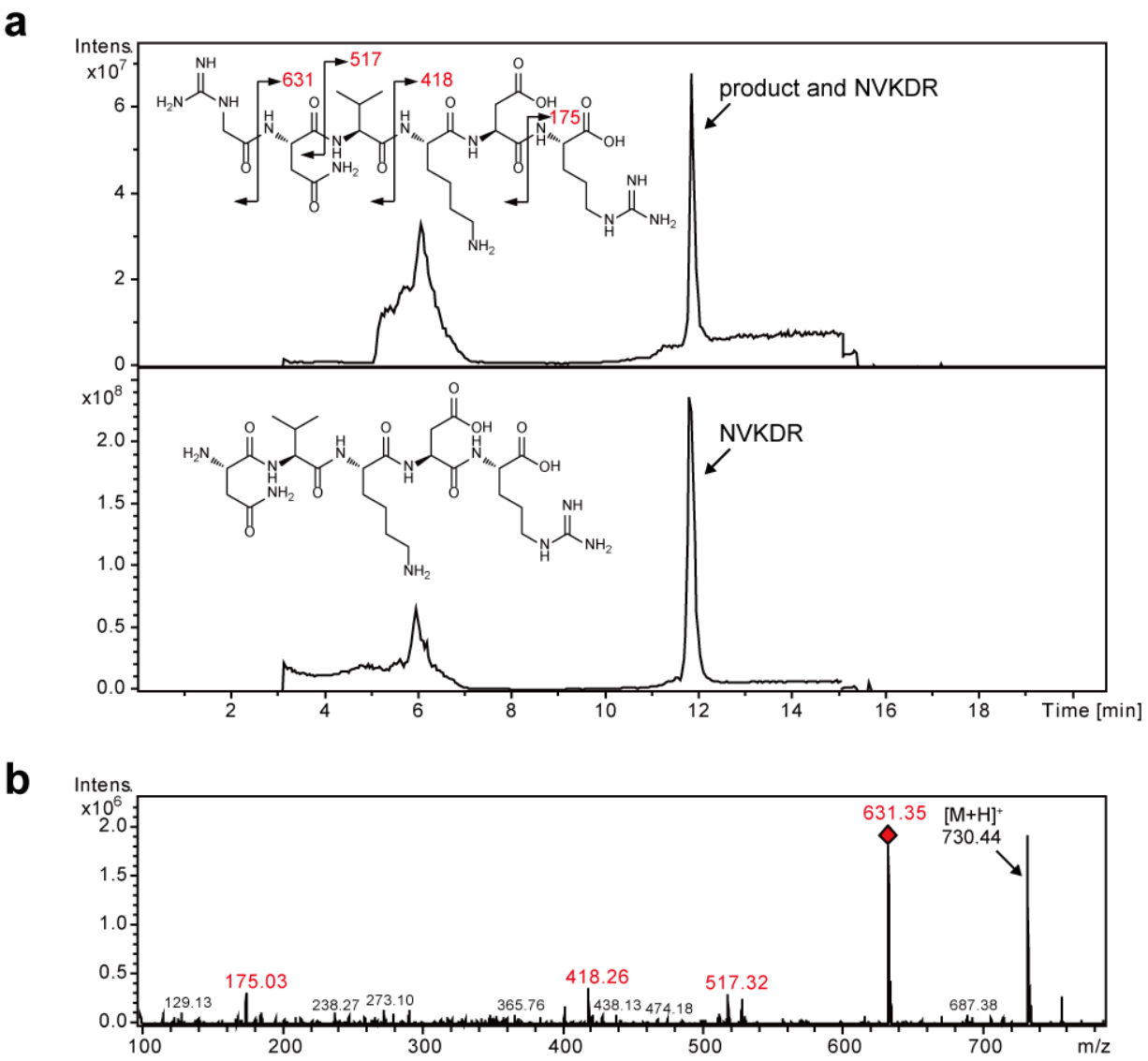

Supplementary Figure 17. LC/ESI-MS analysis of the reaction product. (**a**) Total ion chromatogram of the reaction product formed from 2-guanidinoacetic acid and NVKDR with (upper) and without (lower) PGM1. (**b**) The mass spectrum of the product is shown.

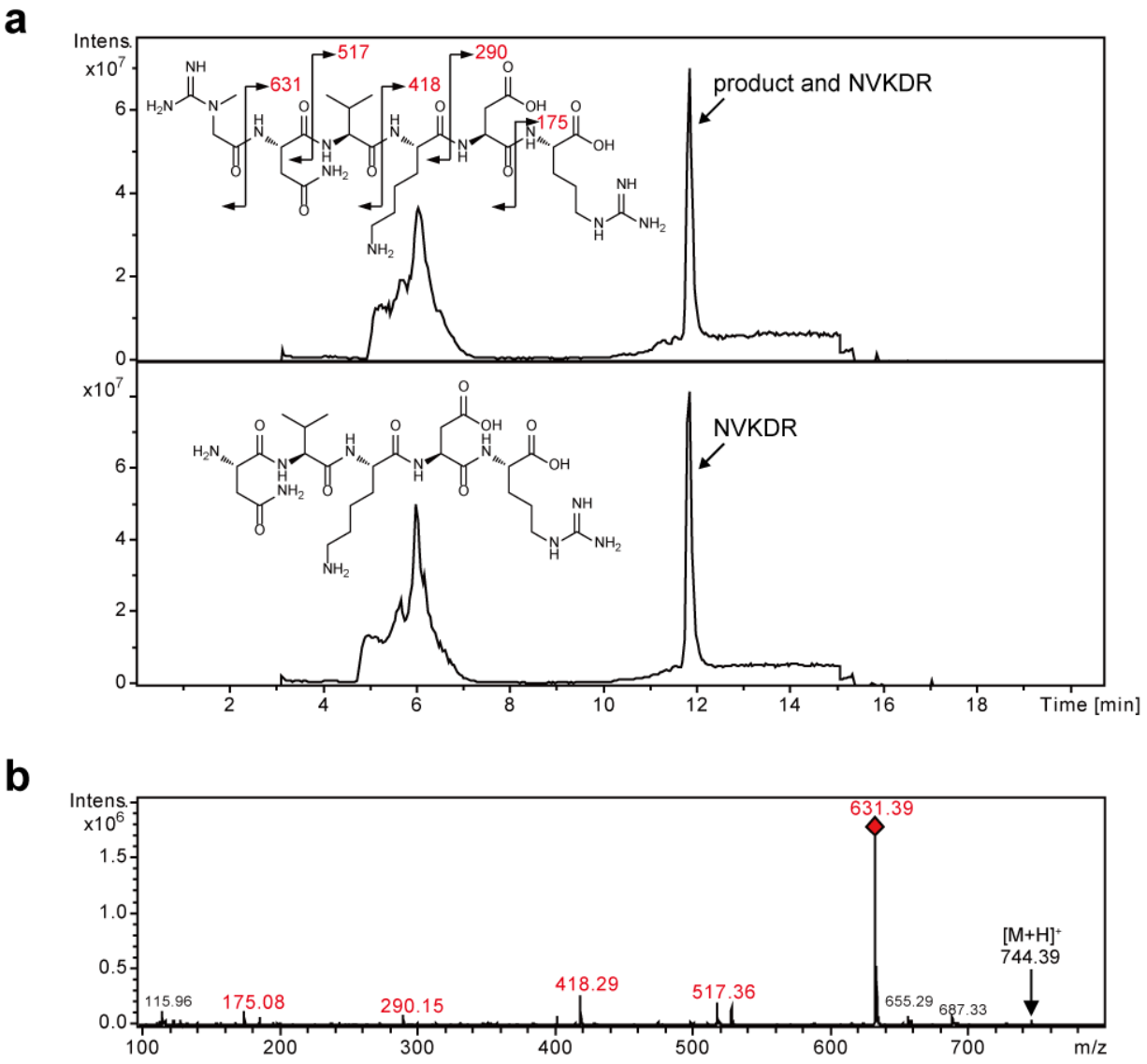

Supplementary Figure 18. LC/ESI-MS analysis of the reaction product. (**a**) Total ion chromatogram of the reaction product formed from creatine and NVKDR with (upper) and without (lower) PGM1. (**b**) The mass spectrum of the product is shown.

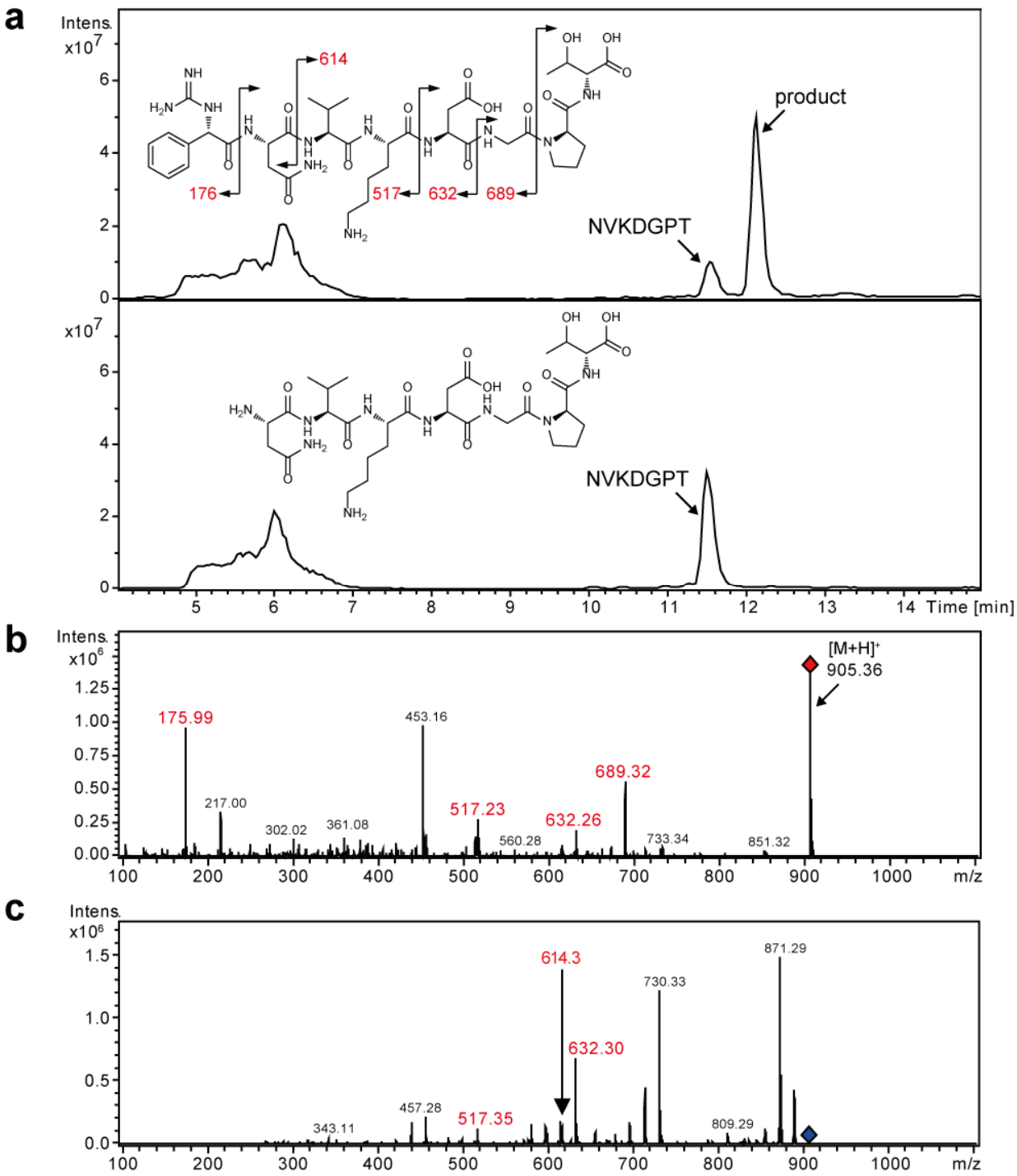

Supplementary Figure 19. LC/ESI-MS/MS analysis of the reaction product. (**a**) Total ion chromatogram of the reaction product formed from **4** and NVKDGPT with (upper) and without (lower) PGM1. (**b** and **c**) The mass spectrum and the MS/MS spectrum of the product are shown, respectively.

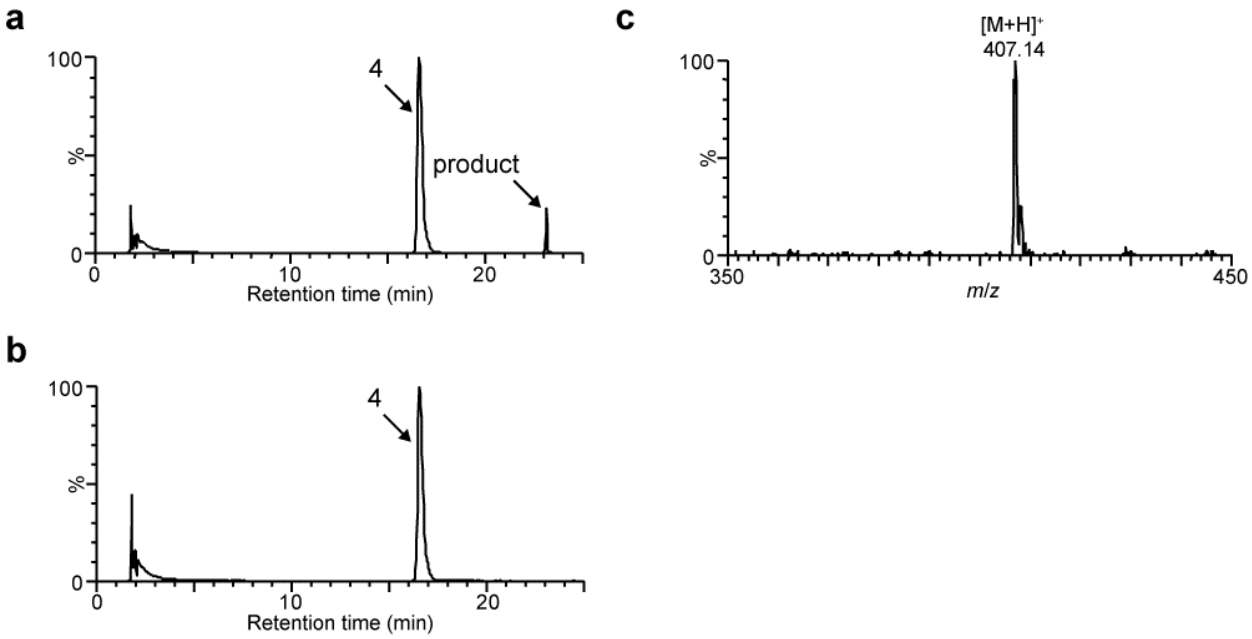

Supplementary Figure 20. LC/ESI-MS analysis of the reaction product. Selected ion chromatogram of the reaction product formed from **4** and NV with (**a**) and without (**b**) PGM1. (**c**) The mass spectrum of the product.

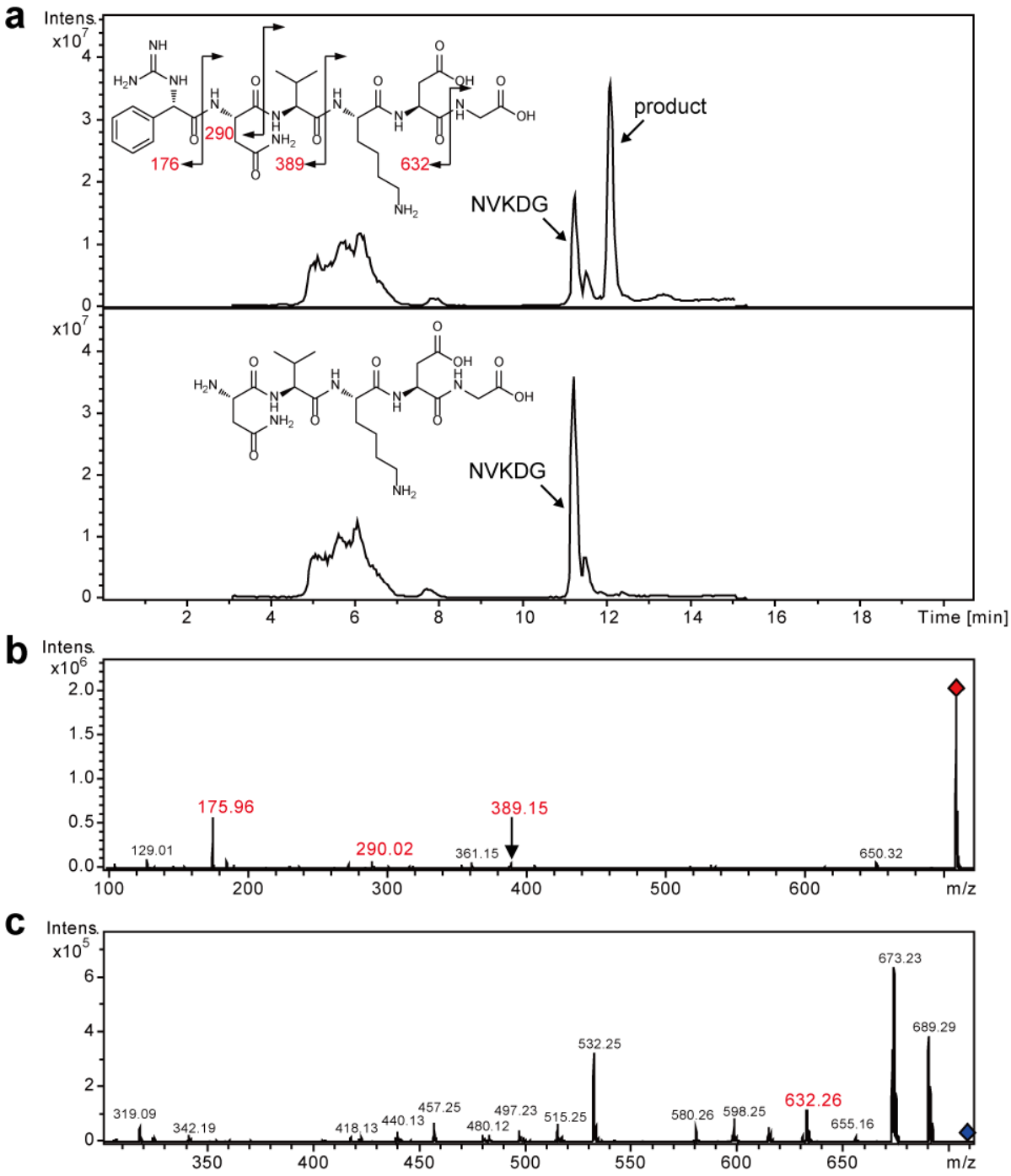

Supplementary Figure 21. LC/ESI-MS/MS analysis of the reaction product. (**a**) Total ion chromatogram of the reaction product formed from **4** and NVKDG with (upper) and without (lower) PGM1. (**b** and **c**) The mass spectrum and the MS/MS spectrum of the product are shown, respectively.

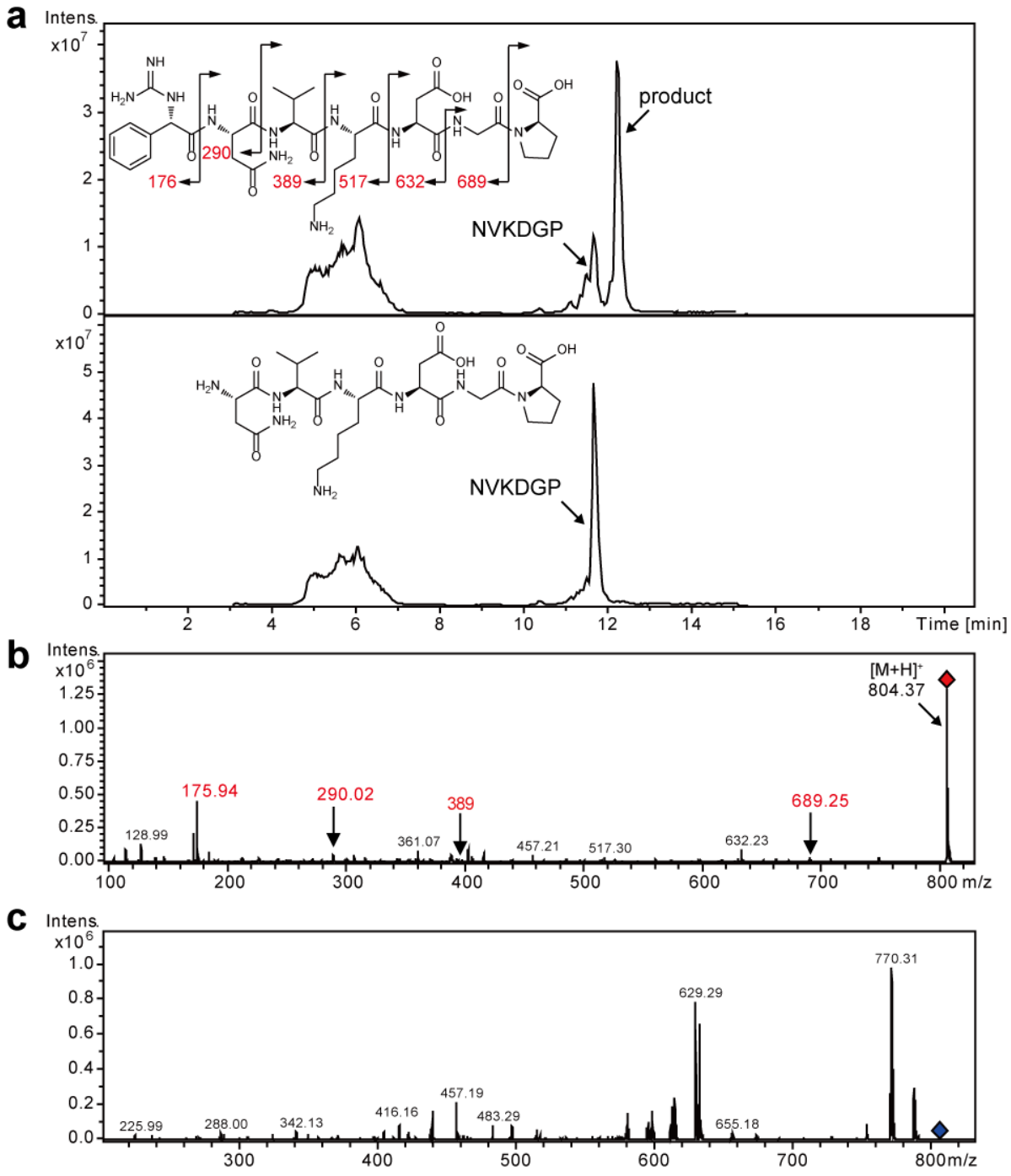

Supplementary Figure 22. LC/ESI-MS/MS analysis of the reaction product. (**a**) Total ion chromatogram of the reaction product formed from **4** and NVKDGP with (upper) and without (lower) PGM1. (**b** and **c**) The mass spectrum and the MS/MS spectrum of the product are shown, respectively.

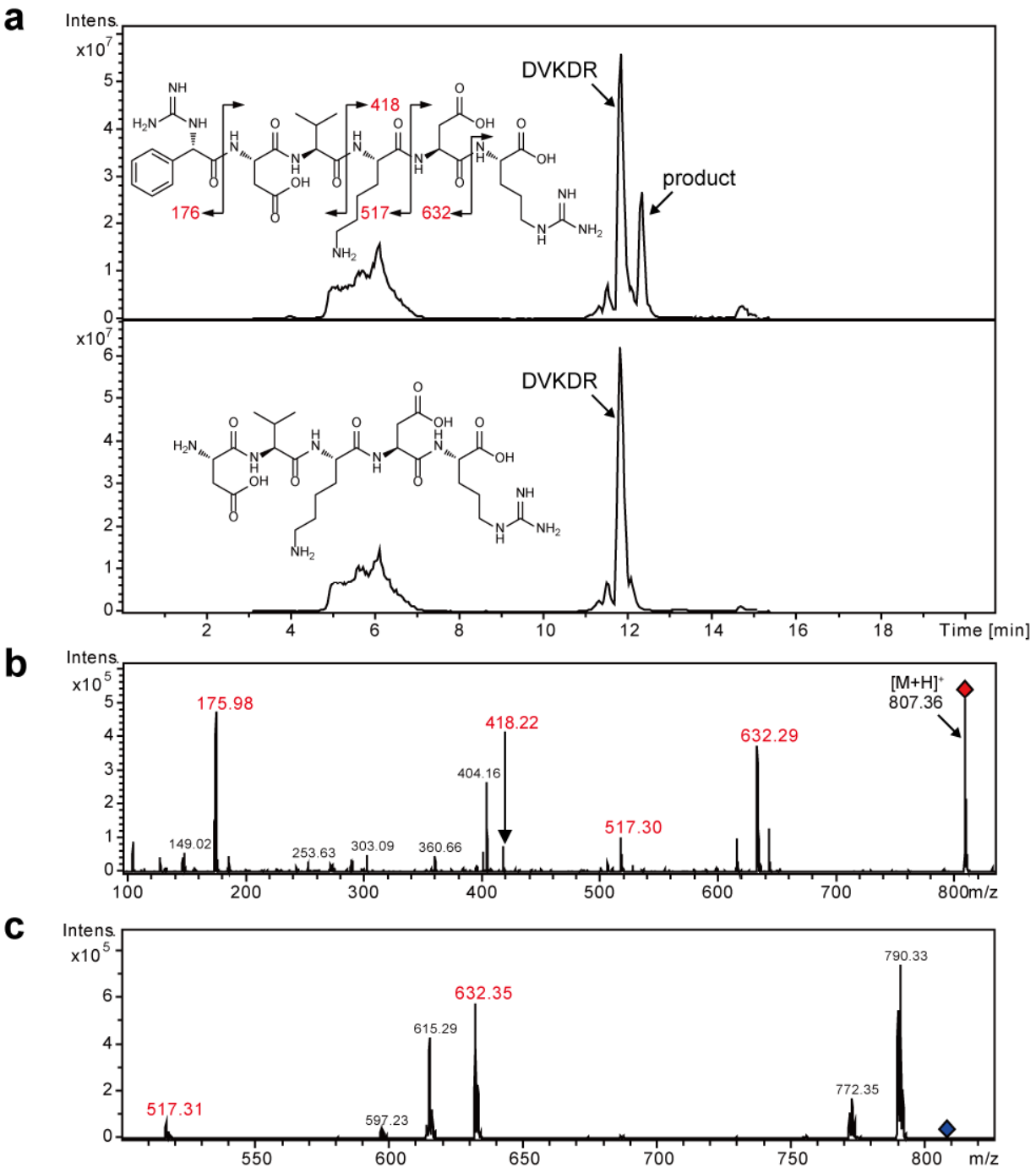

Supplementary Figure 23. LC/ESI-MS/MS analysis of the reaction product. (**a**) Total ion chromatogram of the reaction product formed from **4** and DVKDR with (upper) and without (lower) PGM1. (**b** and **c**) The mass spectrum and the MS/MS spectrum of the product are shown, respectively.

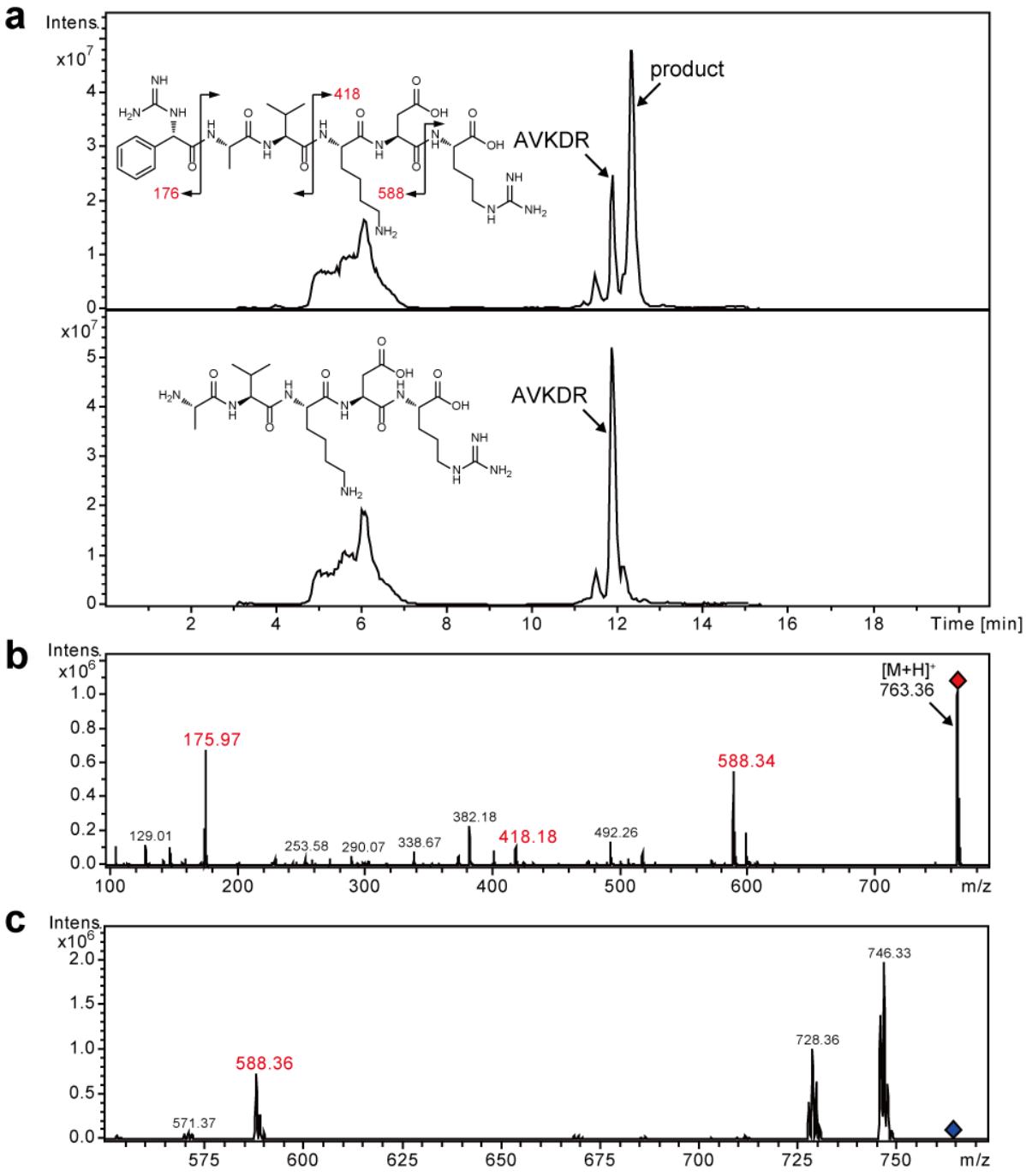

Supplementary Figure 24. LC/ESI-MS/MS analysis of the reaction product. (**a**) Total ion chromatogram of the reaction product formed from **4** and AVKDR with (upper) and without (lower) PGM1. (**b** and **c**) The mass spectrum and the MS/MS spectrum of the product are shown, respectively.

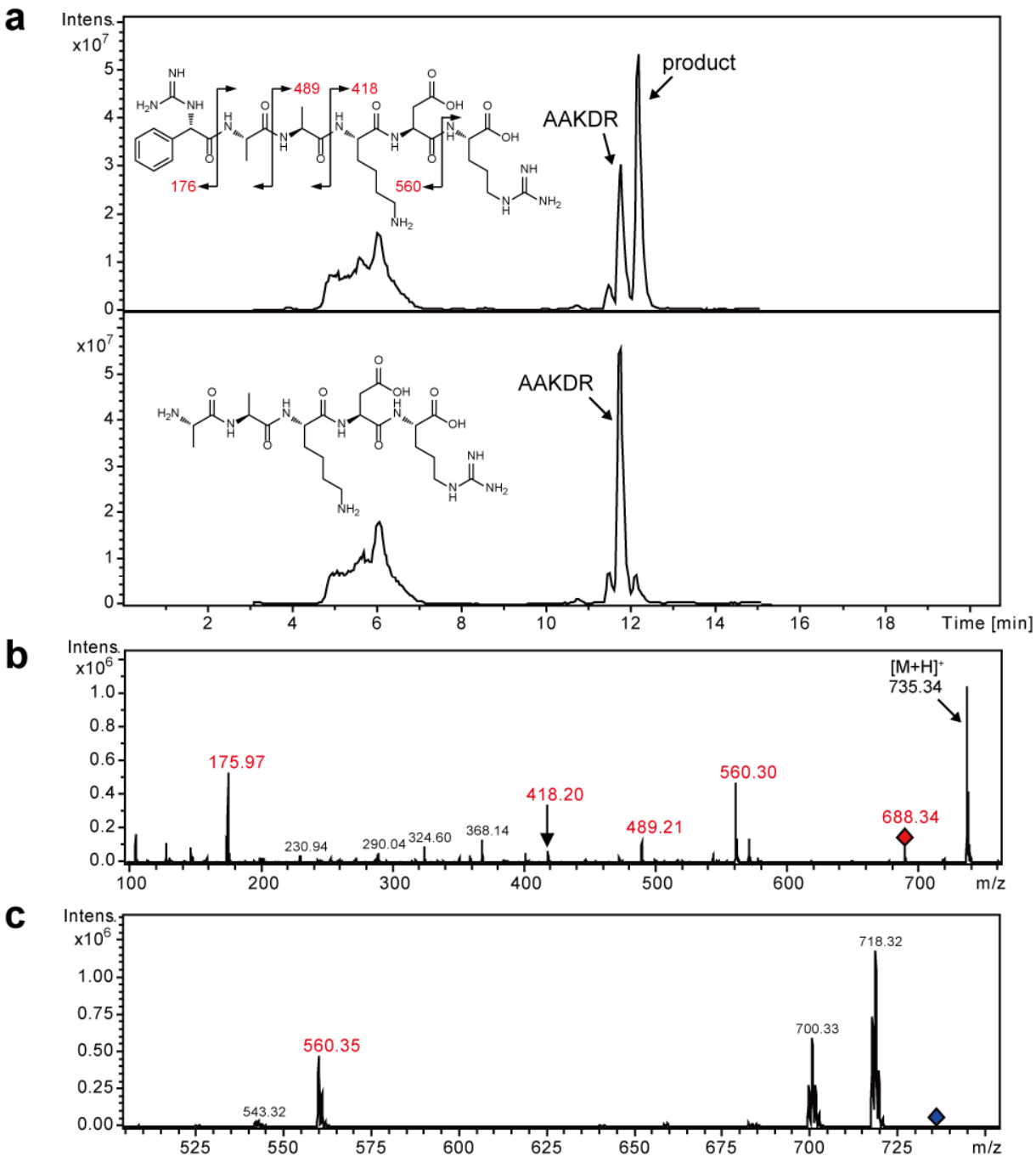

Supplementary Figure 25. LC/ESI-MS/MS analysis of the reaction product. (**a**) Total ion chromatogram of the reaction product formed from **4** and AAKDR with (upper) and without (lower) PGM1. (**b** and **c**) The mass spectrum and the MS/MS spectrum of the product are shown, respectively.

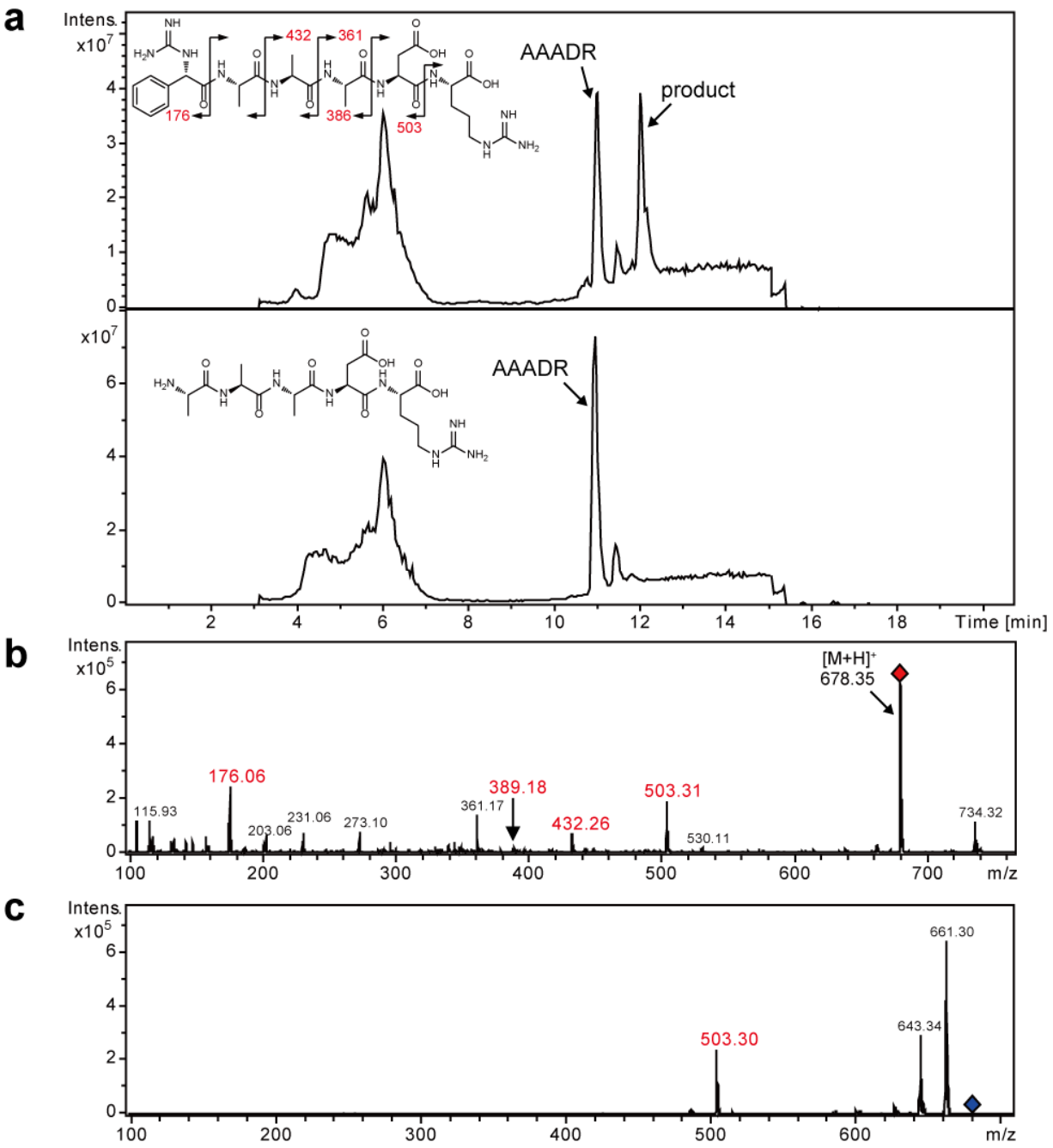

Supplementary Figure 26. LC/ESI-MS/MS analysis of the reaction product. (**a**) Total ion chromatogram of the reaction product formed from **4** and AAADR with (upper) and without (lower) PGM1. (**b** and **c**) The mass spectrum and the MS/MS spectrum of the product are shown, respectively.

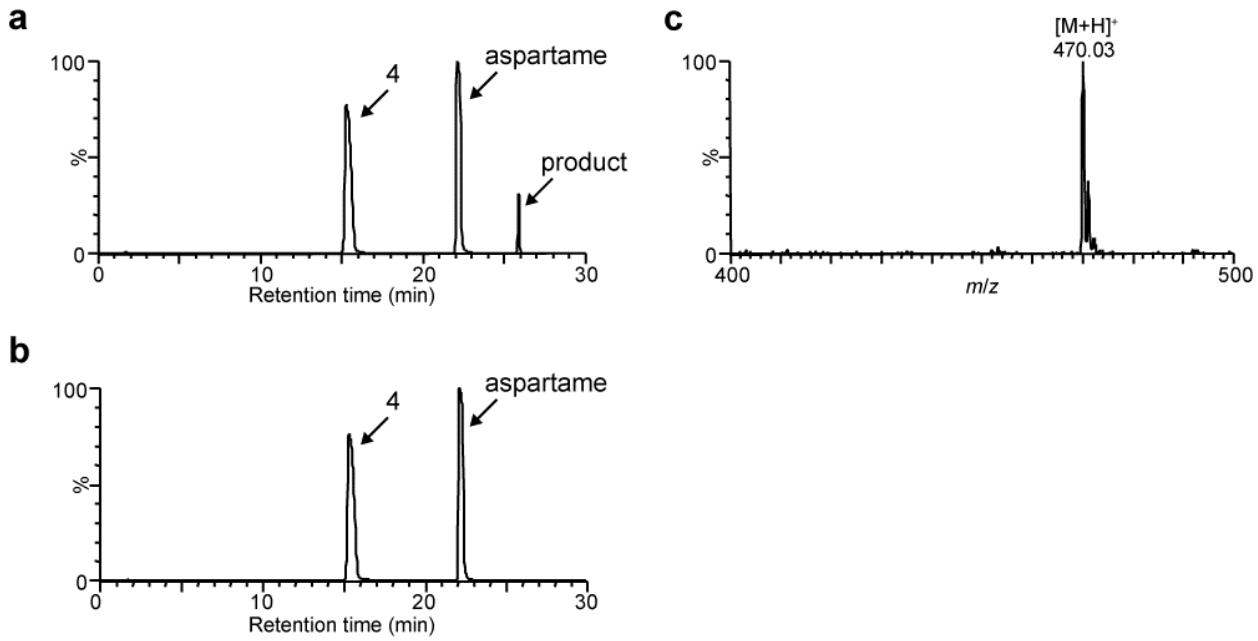

Supplementary Figure 27. LC/ESI-MS analysis of the reaction product. Selected ion chromatogram of the reaction product formed from **4** and aspartame with (**a**) and without (**b**) PGM1. (**c**) The mass spectrum of the product.

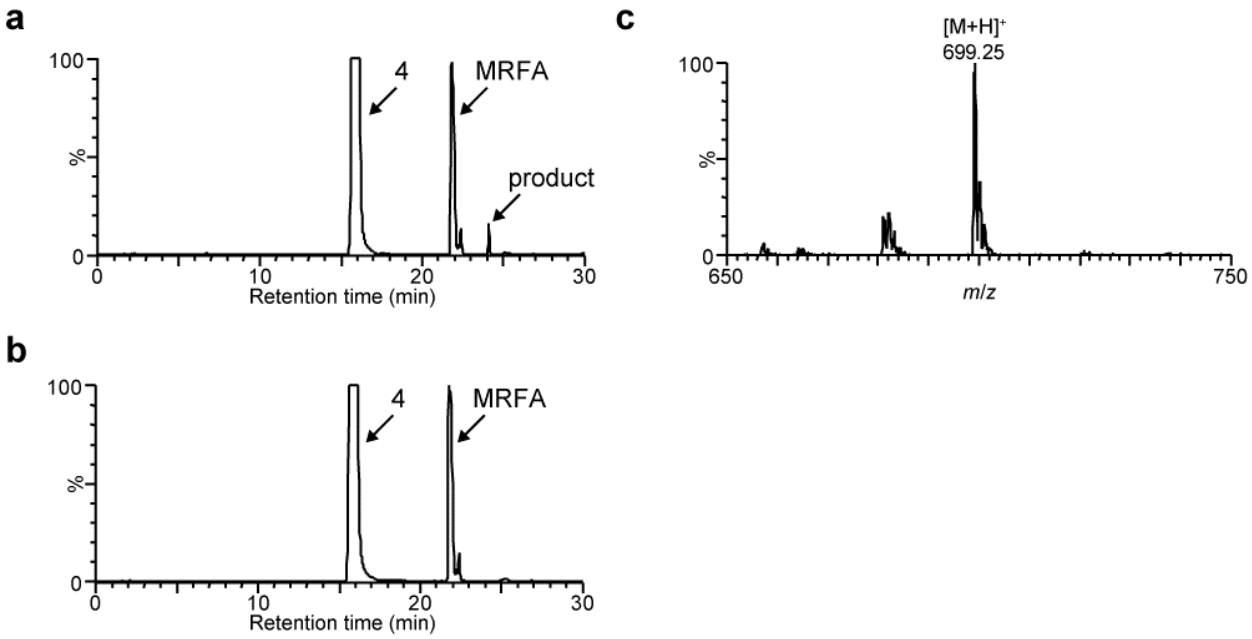

Supplementary Figure 28. LC/ESI-MS analysis of the reaction product. Selected ion chromatogram of the reaction product formed from **4** and MRFA with (**a**) and without (**b**) PGM1. (**c**) The mass spectrum of the product.

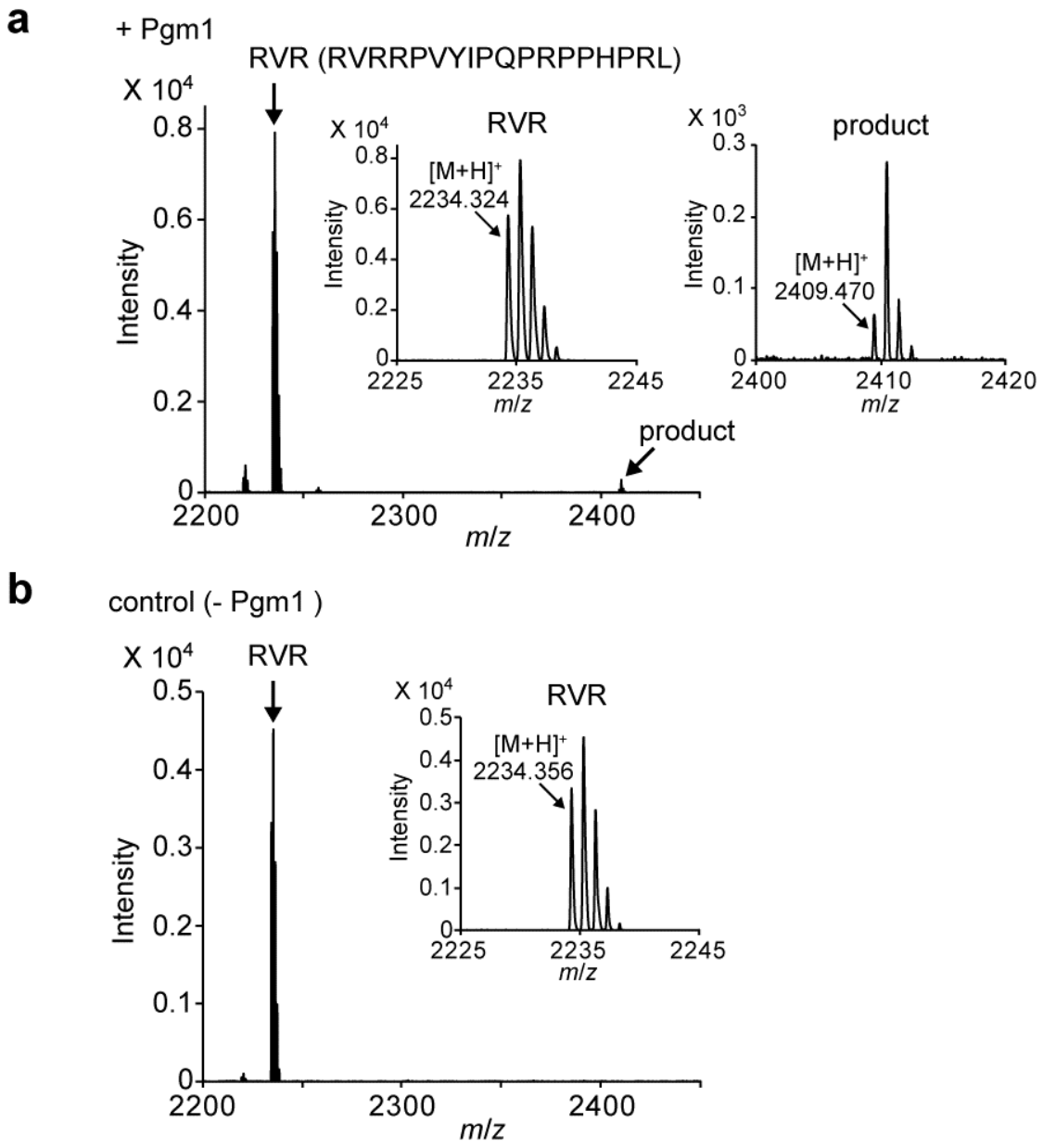

Supplementary Figure 29. MALDI-TOF-MS analysis of the reaction products formed from 4 and the apidaecin derivative, RVR, catalyzed by PGM1. MALDI-TOF-MS analysis of the reaction products formed from **4** and apidaecin derivative RVR with (**a**) and without (**b**) PGM1.

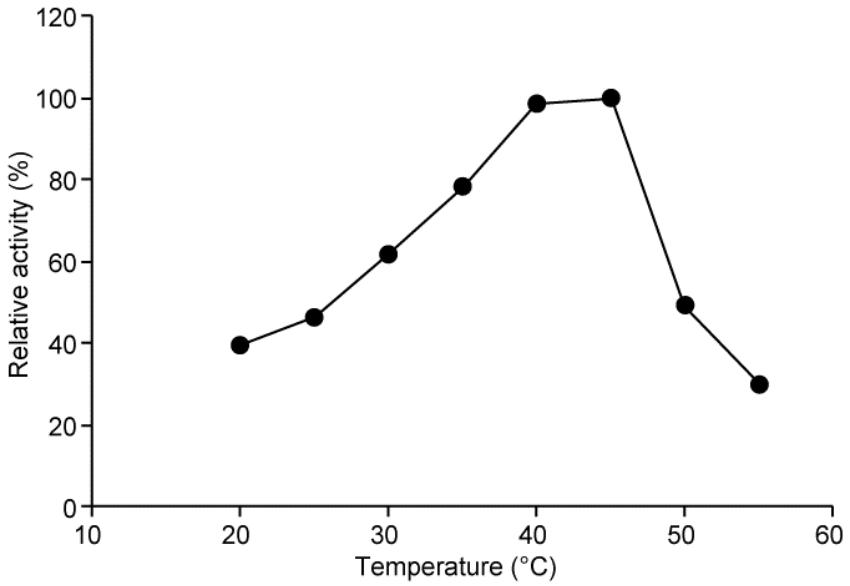

Supplementary Figure 30. Effects of temperature on PGM1 activity. The assay was conducted from 20 to 55°C. The assay mixture contained in a final volume of 100 μL was 50 mM Tris-HCl, pH 8.0, 50 μM NVKDR, 50 μM **4**, 5 mM ATP, 5 mM Mg^{2+}, and 4 μg of PGM1. The mixture was incubated at 30°C for 5 min. Average value obtained by two independent experiments was shown. Values were within 8.2 percent of each other.

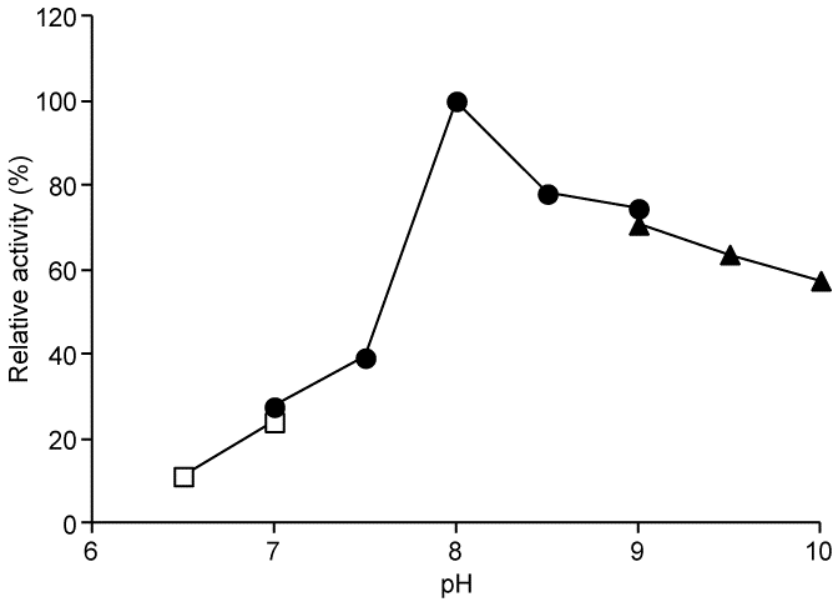

Supplementary Figure 31. Effects of pH on PGM1 activity. The assay was conducted from pH 6.5 to 10 using 50 mM MES (open squares), 50 mM Tris-HCl (solid circles), and 50 mM glycine-NaOH buffer (solid triangles). The assay mixture in each of the buffer contained in a final volume of 100 μL was 50 μM NVKDR, 50 μM **4**, 5 mM ATP, 5 mM Mg^{2+}, and 4 μg of PGM1. The mixture was incubated at 30°C for 5 min. Average value obtained by two independent experiments was shown. Values were within 8.5 percent of each other.

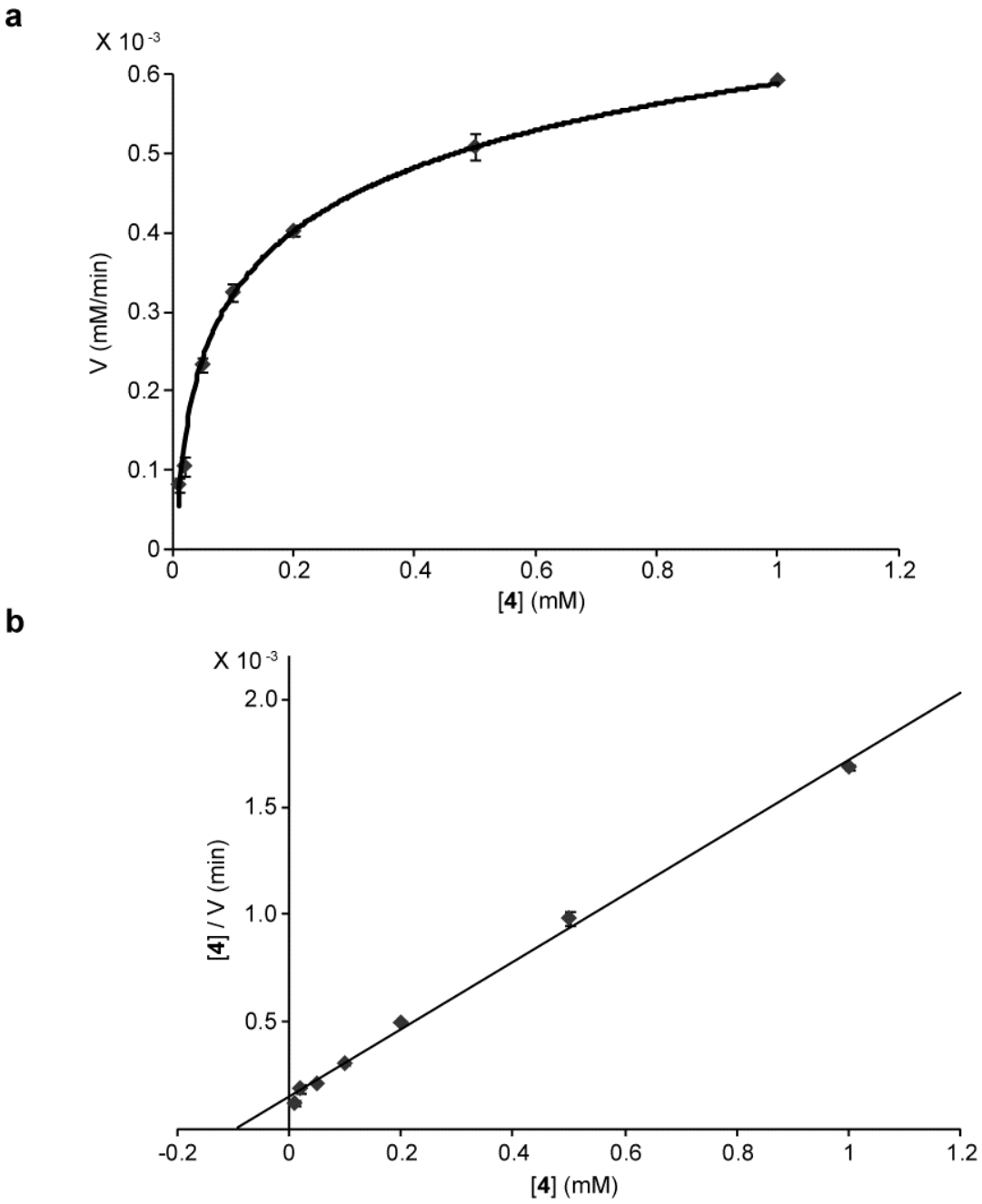

Supplementary Figure 32. Michaelis-Menten plot (a) and Hanes-Woolf plots (b) of the PGM1 catalyzed reaction of 0.5 mM peptide NVKDR and varied concentrations of 4. Triplicate sets of enzyme assays were performed at each substrate concentration. Values were within 9.0 percent of each other.

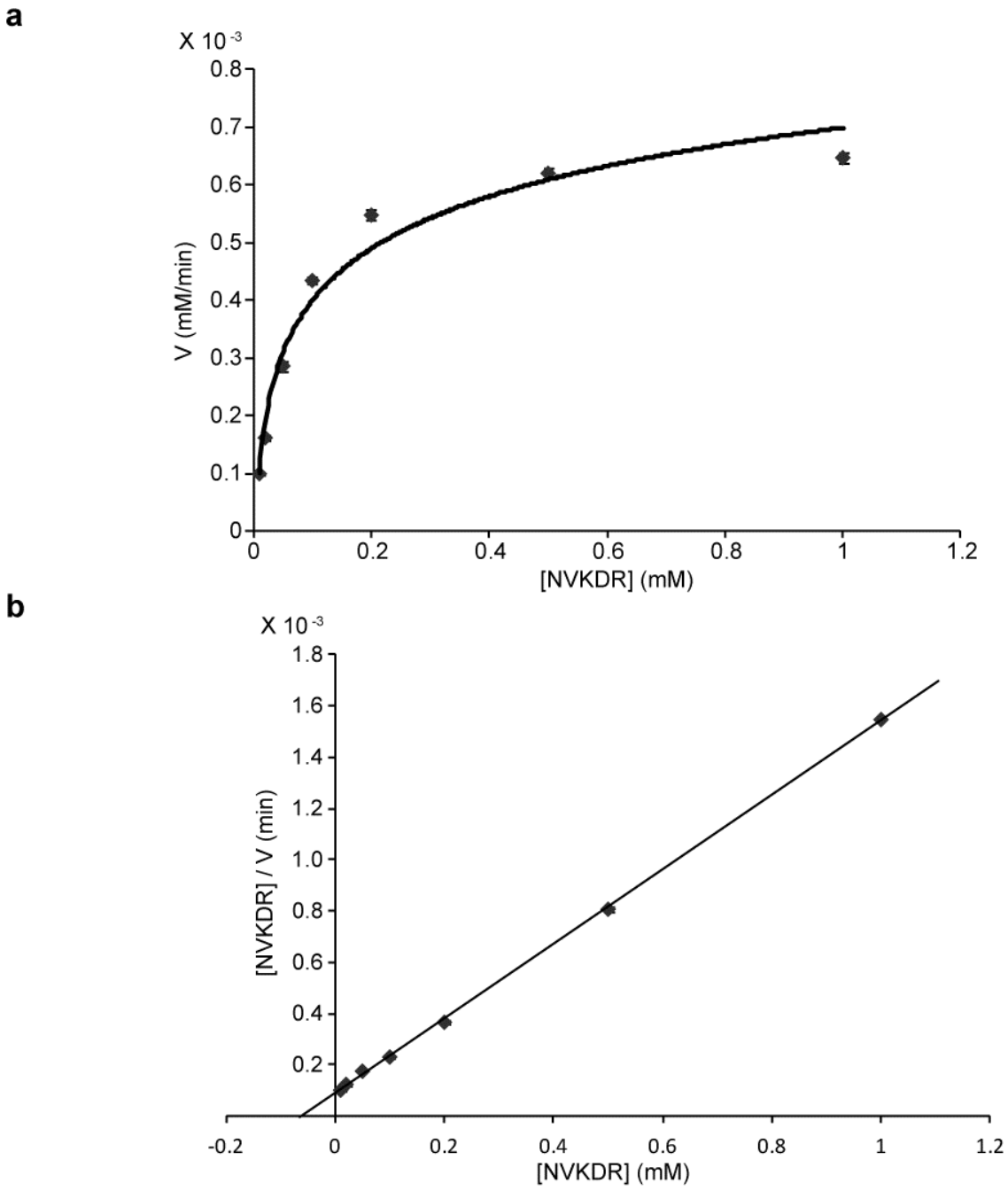

Supplementary Figure 33. Michaelis-Menten plot (a) and Hanes-Woolf plots (b) of the PGM1 catalyzed reaction of 0.5 mM of 4 and varied concentrations of NVKDR. Triplicate sets of enzyme assays were performed at each substrate concentration. Values were within 4.6 percent of each other.

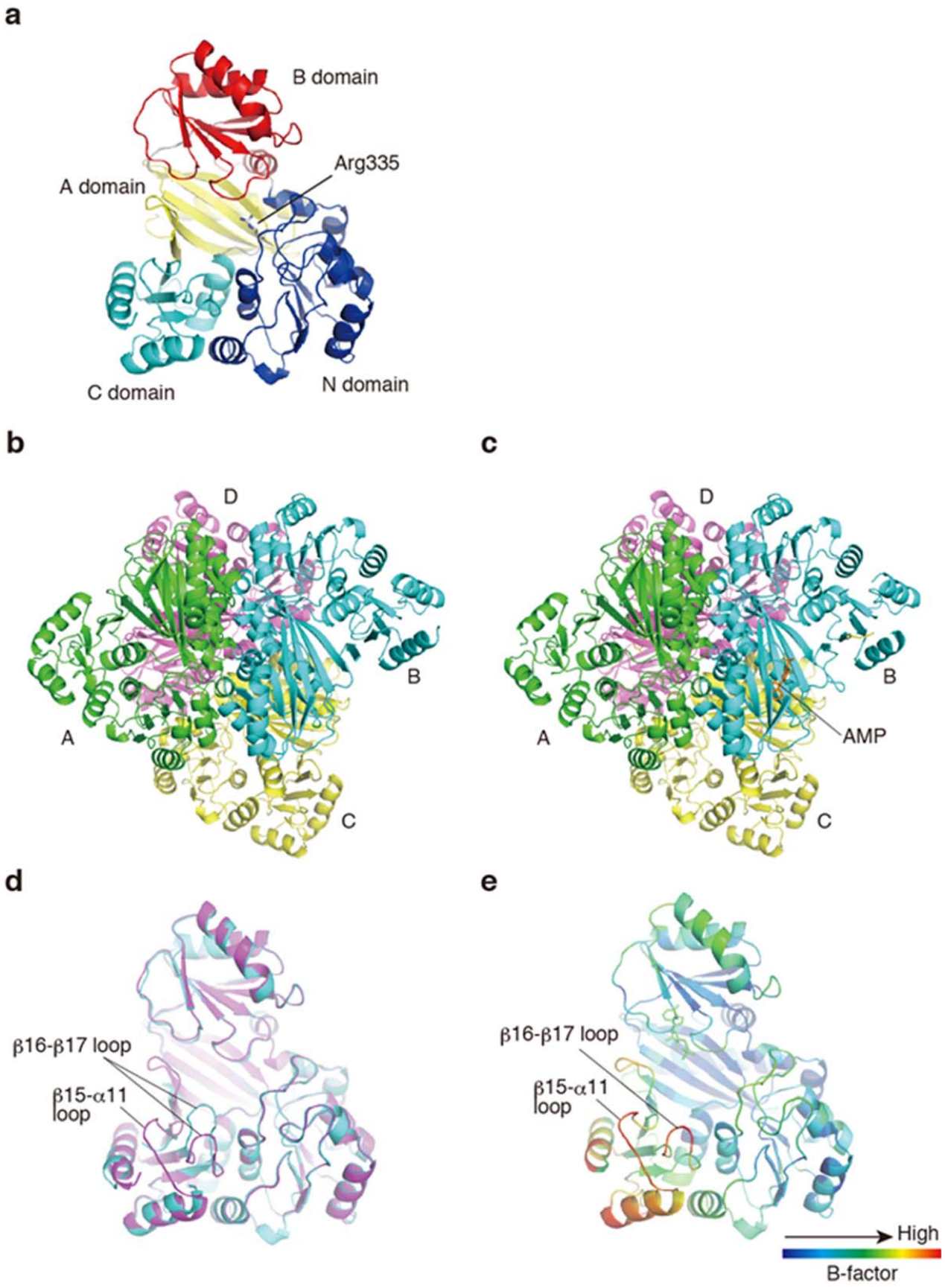
a
B domain
Arg335
A domain
C domain
N domain
b
D
B
A
C
c
D
B
A
AMP
C
d
β16-β17 loop
β15-α11 loop
e
β16-β17 loop
β15-α11 loop
High
B-factor

Supplementary Figure 34. Overall structure of PGM1 in asymmetric unit. (a) Crystal structure of PGM1 apo is shown in cartoon model. The N, A, B and C domains are colored in blue, yellow, red and cyan, respectively. The AMP molecule and Arg335 are represented with green and light brown stick models, respectively. (**b** and **c**) Four monomers in the asymmetric unit of PGM1 apo (**b**) and AMP complex (**c**) are shown. Monomers A, B, C and D are colored in green, cyan, yellow and magenta, respectively. The AMP molecules are indicated with an orange stick model. A/B and C/D form two sets of biologically active, symmetric dimers. The electron density of the β- and γ-phosphates of AMPPNP in monomers B, C and D are weak or disordered respectively, despite the use of the ATP analogue, AMPPNP, for the crystallization. The electron density of AMPPNP in monomer A was not observed. Thus, only the AMP molecule was put in monomers B, C and D in the crystal structure of PGM1. Each monomer in PGM1 apo and AMP complex showed root-mean-square deviation (r.m.s.d.) of 1.83–2.41 Å and 0.35–0.52 Å for Cα-atoms, respectively. (**d**) The overlay of the overall structures of monomers B and D in the PGM1 apo structure is shown. Each molecule is indicated according to (**b**). Significant backbone changes were observed at β15–α11 (residues 364–373) and β16–β17 (339–411) of monomer B in the apo structure. (**e**) The B-factor of the PGM1-AMP complex is shown. The C domain has high B-factors, indicative of a high degree of flexibility.

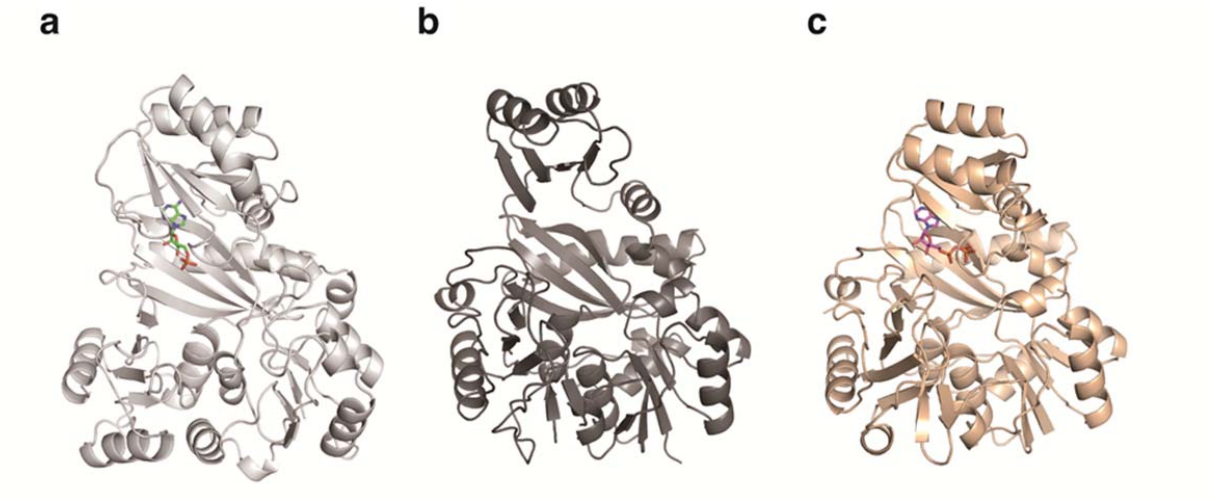

Supplementary Figure 35. Comparison of overall structure of PGM1, *E. coli* PurD, and *A. aeolicus* PurD. The crystal structures of (**a**) PGM1-AMP complex, (**b**) *E. coli* PurD apo (PDB entry 1GSO), and (**c**) *A. aeolicus* PurD-ATP complex (PDB entry 2YW2) are shown in white, gray and wheat cartoon models, respectively. AMP in PGM1 and ATP in *A. aeolicus* PurD are indicated with green and magenta stick models, respectively.

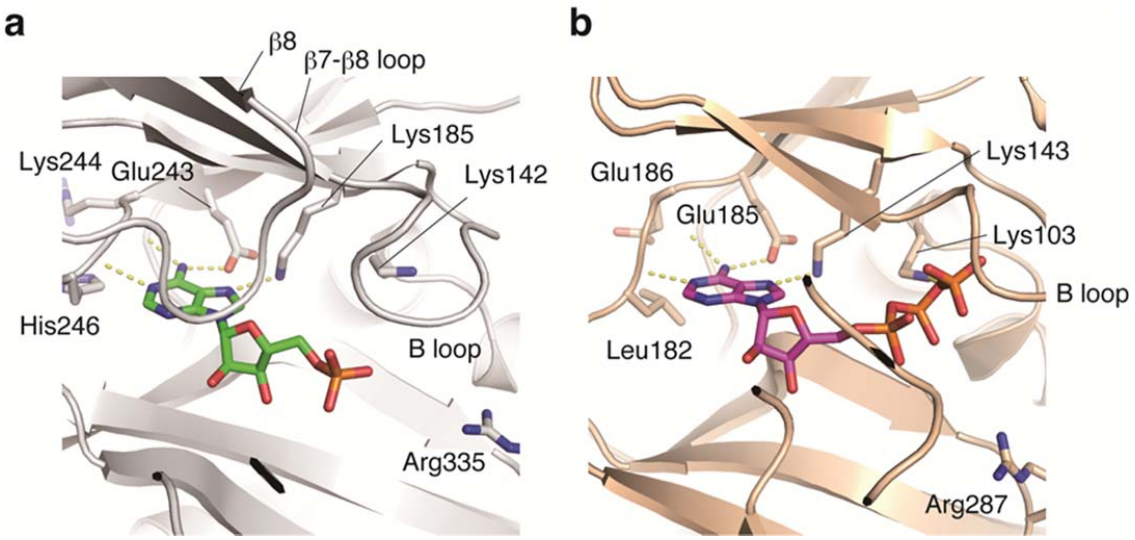

Supplementary Figure 36. Comparison of the ATP-binding site of PGM1 and *A. aeolicus* PurD. Close-up views of the ATP-binding site of (**a**) PGM1-AMP complex and (**b**) *A. areolicus* PurD-ATP complex (PDB entry 2YW2) are shown with the conserved residues between the enzymes. AMP in PGM1 and ATP in *A. aeolicus* PurD are represented with green and magenta stick models. The hydrogen bonds are indicated with dotted lines. The adenine ring of AMP is locked deep inside the ATP-binding site. The AMP molecule is located in a nearly identical position, except for the α-phosphate. PGM1 has a β7–β8 loop (residues 200–210) and a β8 strand (residues 211–214) on the B domain, while PurD does not have these structures. These loops and B-loop in PGM1 shift toward the inside of the ATP-binding site.

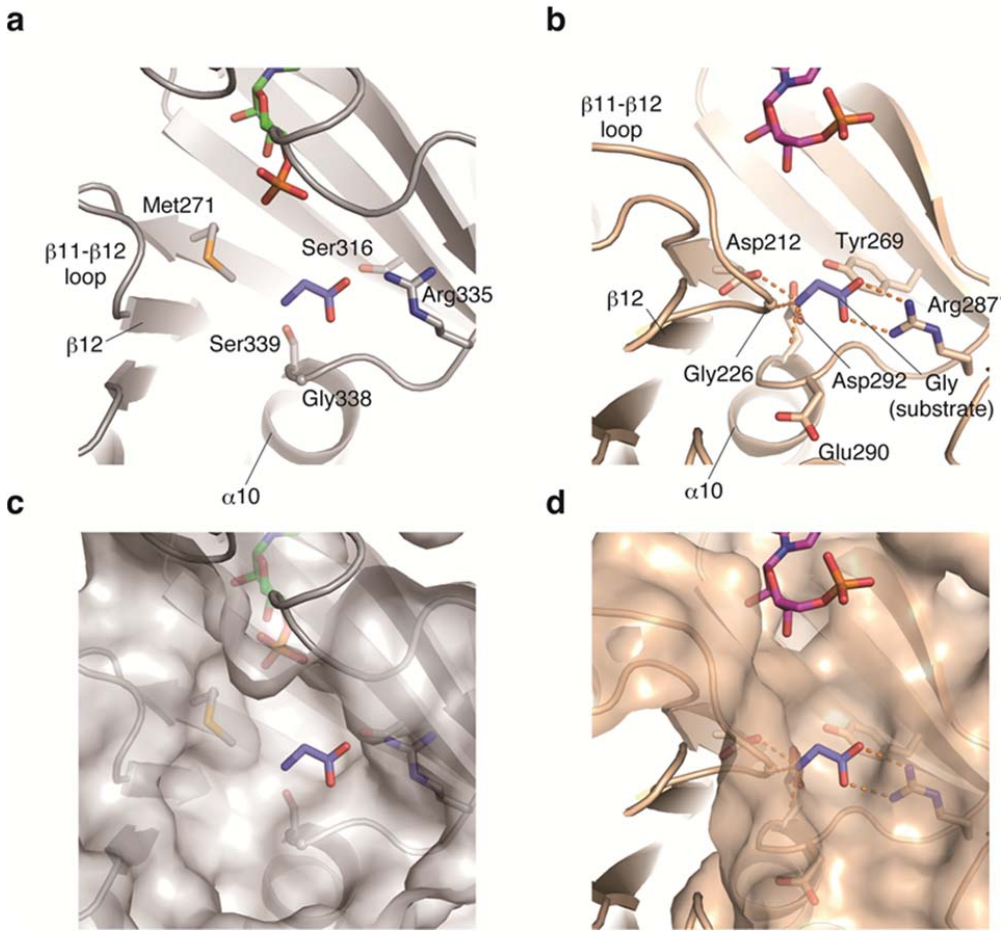

Supplementary Figure 37. Comparisons of the *N*-terminus substrate-binding site of PGM1 and *Geobacillus kaustophilus* PurD. Close-up views of the *N*-terminus substrate-binding site of (**a** and **c**) PGM1-AMP complex and (**b** and **d**) *G. kaustophilus* PurD-AMP-glycine complex (PDB entry 2YS6) are shown by (**a** and **b**) cartoons and (**c** and **d**) surface models. AMP molecules bound to PGM1 and *G. kaustophilus* PurD, and glycine bound to *G. kaustophilus* PurD are indicated in green, magenta and blue stick models, respectively. The glycine molecule in PurD is also superimposed on PGM1. The hydrogen bonds are indicated with dotted lines. The β11–β12 loop (residues 213–228) including the three glycine-bound residues, Gly226, Asp 212 and Lys214, in *G. kaustophilus* PurD are replaced with the short loop β11–β12 (residues 272–279) in PGM1. The α10 helix (residues 339–351) and β12 strand (residue 279–282) in the N and C domains are displaced by 1.5 Å and 4.5 Å toward the outside of the substrate binding site, respectively, compared with those of *G. kaustophilus* PurD. Large-to-small

Tyr/Asp substitutions with Ser at position 316 and 339 in PGM1 opens a space deep inside the binding site. These conformational differences expand the substrate binding site of PGM1.

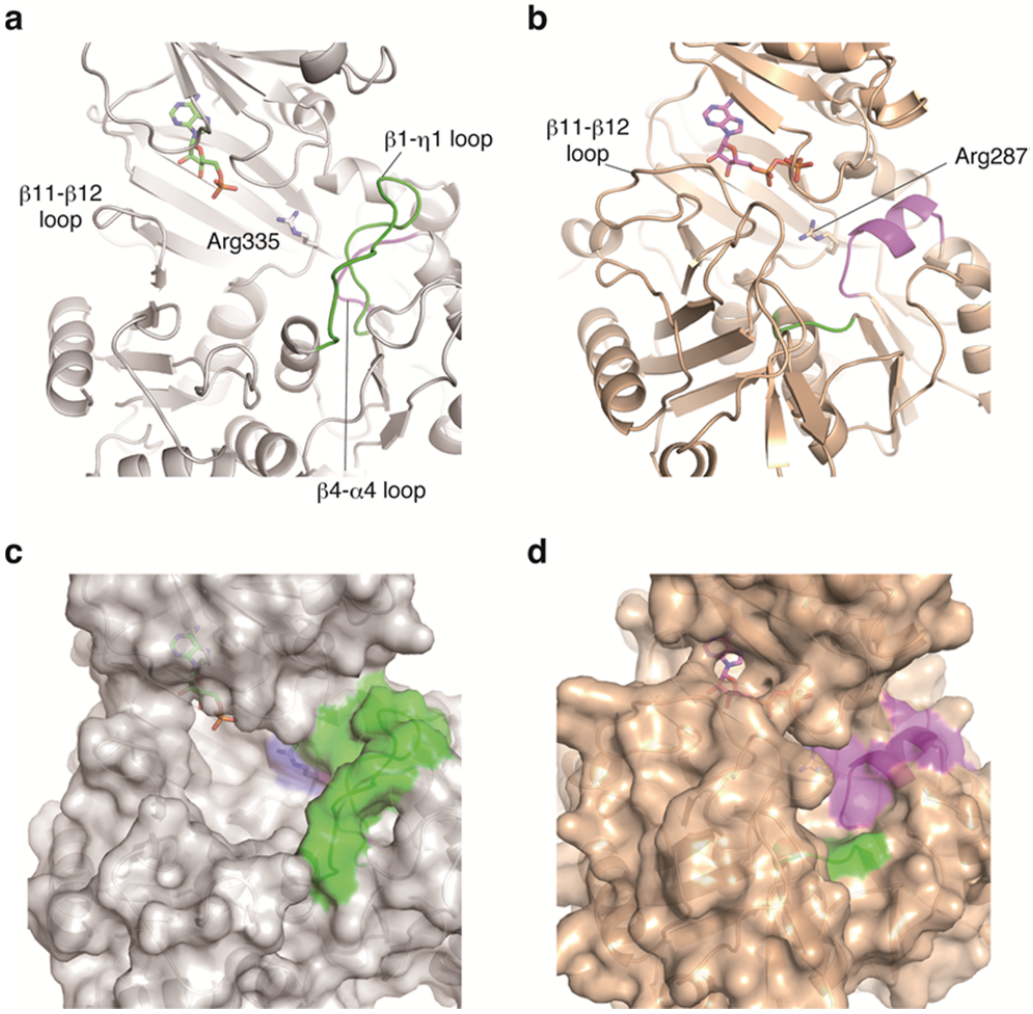

Supplementary Figure 38. Comparison of the cleft of PGM1 and the corresponding region in PurD. Close-up views of the cleft of (**a** and **c**) PGM1-AMP complex and the corresponding region in (**b** and **d**) *A. areolicus* PurD-ATP complex (PDB entry 2YW2) are shown with (**a** and **b**) cartoons and (**c** and **d**) surface models. Arg335 in PGM1 and the corresponding Arg in PurD are indicated with stick models. The position of Arg335 is highlighted in blue in the surface model of PGM1. AMP and ATP molecules bound to PGM1 and PurD are indicated by green and magenta stick models. The β4–α4 loop (residues 105–109) in PGM1 and the corresponding α-helix in PurD are colored in magenta. The β1–η1 loop (residues 8–20) in PGM1 and the corresponding loop in PurD are colored in green. The α-helix (residues 69–77) and loop (residues 8–10) in the N domain in PurD are replaced with a shorter β4–α4 loop and much longer β1–η1 loop in PGM1, respectively. Thus, the β1–η1 loop lies on the β4–α4 loop and creates the characteristic long cleft in PGM1.

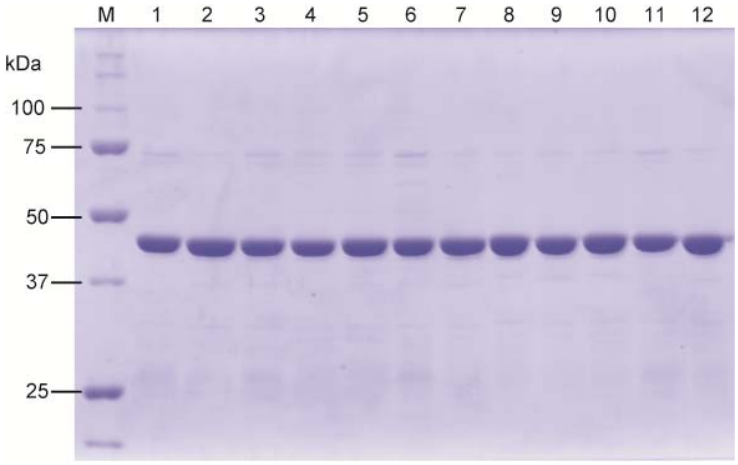

Supplementary Figure 39. SDS-PAGE of mutant PGM1 enzymes. M, molecular mass marker; lane 1, A14R; lane 2, A14Q; lane 3, A14L; lane 4, S190L; lane 5, S190A; lane 6, E255D; lane 7, E255S; lane 8, S316D; lane 9, R335M; lane 10, R335Q; lane 11, R335N; lane 12, S339A.

References

1. Waldrop, G.L., Rayment, I. & Holden, H.M. Three-dimensional structure of the biotin carboxylase subunit of acetyl-CoA carboxylase. *Biochemistry* **33**, 10249-10256 (1994).

2. Yamaguchi, H. *et al*. Three-dimensional structure of the glutathione synthetase from *Escherichia coli* B at 2.0 A resolution. *J. Mol. Biol.* **229**, 1083-1100 (1993).

3. Kim, J.H., Krahn, J.M., Tomchick, D.R., Smith, J.L. & Zalkin, H. Structure and function of the glutamine phosphoribosylpyrophosphate amidotransferase glutamine site and communication with the phosphoribosylpyrophosphate site. *J. Biol. Chem.* **271**, 15549-15557 (1996).